Materials and Methods

E1E2 and antibody constructs

The AMS0232 E1E2 sequence was obtained from an HIV-1 infected individual from the MOSAIC cohort study (*32*). The full-length amino acid E1E2 sequence (amino acids 192-746, H77 numbering) (*60*) was codon-optimized for expression in human cell lines and cloned into the pPPI4 expression vector downstream of a custom signal peptide (MDAMKRGLCCVLLLCGAVFVSVTG). StrepII-tagged AMS0232 E1E2 was generated by replacing amino acids 384-396 in the hypervariable region 1 (HVR1) of E2 by a strepII-tag (SAWSHPQFEK). Mutations in AMS0232 E1E2 were introduced using the QuickChange II Site-directed mutagenesis kit (Agilent) or Q5 Site-Directed mutagenesis kit (New England Biolabs).

Amino acid sequences of the antibody variable heavy (VH) and light chains (VL) were codon-optimized and cloned into IgG1 in mammalian expression vectors. The StrepII-tagged heavy chain (HC) Fab of AR4A was generated by introducing a Gly-Gly-Ser-linker followed by a StrepII-tag directly downstream of the cysteine that pairs with the light chain (LC). For the production of the CrossFab, we generated an AT1209 VL-CH construct by fusing the VL to the heavy constant domain (CH) of IgG1 Fab and an AT1209 VH-CL construct by fusing the VH to the constant light (CL) domain separated by elbow regions as described by Schaefer and colleagues (*37*). CDR loops and antibody amino acids are defined according to Kabat nomenclature and numbering scheme.

Antibody and Fab production

All proteins were transiently transfected in suspension HEK293F cells (Invitrogen, cat no. R79009) maintained in Freestyle medium (Life Technologies). For antibody production, HEK293F were grown to a density of ~1.0 x 10^6 cells/ml and were co-transfected with heavy chain (HC) and (LC) plasmids (1:1) mixed with PEIMAX (Polysciences). After five days, the supernatant was harvested, filtered and the antibodies were purified using protein G or protein A agarose resin (Pierce) according to manufacturer's instruction. The eluted antibodies were

concentrated in PBS and injected in a Superdex200 Increase column equilibrated in PBS. Peak fractions were collected and concentrated with Vivaspin6 10-kDa cutoff filters. To produce IGH505 Fab, we incubated purified IGH505 IgG1 with papain-resin (Thermo Fisher) in digestion buffer (PBS + 20 mM Cysteine-HCL+ 10 mM EDTA, pH = 7.4) for 5 h at 37°C. We stopped the reaction by centrifuging the mix in a Spin-X centrifuge and removed residual IgG1 and Fc fragments by incubating the flow-through with protein A agarose for 2 h at room temperature. Flow-through was injected into a Superdex200 column and peak fractions corresponding to IGH505 Fab were collected and concentrated in Vivaspin6 10-kDa filter units. The polyclonal IgG serum pool used in Figure 1a consist of serum samples from four $HCV^{+}HIV^{+}$ individuals of the MOSAIC cohort. The two serum pools were diluted 1:4 in PBS before purification with protein G or protein A agarose resin (Pierce) according to manufacturer's instruction. The eluted polyclonal IgG serum was then concentrated with a Vivaspin6 10-kDa cutoff filters, volume was adjusted to match the input serum volume using PBS and stored at 4°C.

Pseudoparticle infectivity and neutralization assays

To generate pseudoparticles (HCVpp), 293T or 293T CD81KO cells were co-transfected with three plasmids: a MLV (phCMV-5349) packaging construct, a luciferase reporter plasmid and an expression vector encoding the full-length H77 E1E2 or AMS0232 E1E2 and its mutants (*60*). Supernatants containing HCVpp were collected after 72 h and stored at -80°C until further use. To compare infectivity between wild type and mutant HCVpp, the supernatants were added to Huh-7 cells, incubated for 4h before addition of DMEM culture media. Luciferase signal was measured after 72 h. For neutralization studies, pseudovirus-containing supernatant was incubated in duplicates or quadruplicates with a dilution series of purified polyclonal human IgG or mAbs prior to infection. Virus-antibody mixtures were incubated for 1 h at 37 °C and were added to Huh-7 cells and incubated for 4 h before addition of DMEM culture media. Infection was allowed to proceed for 72 h. For all readouts, the samples were lysed and assayed using Firefly luciferase and a GloMax luminometer (Promega, USA). Data was analysed in GraphPad Prism 8.0.

ELISA

Purified E1E2 + AR4A-StrepII complexes (1.0 μg ml^{-1} in TBS with 0.1% DDM) were coated for 2 h at room temperature on 96-well Strep-Tactin XT coated microplates (IBA LifeSciences). Plates were washed twice with TBS/0.05% Tween20 before incubating with serially diluted mAbs and CD81-LEL-hFc (R&D systems) in casein blocking buffer (Thermo Fisher Scientific) diluted 1:1 v:v in TBS with 0.1% DDM (casein/0.05% DDM) for 90 min. After three washes with TBS/0.05% Tween20, HRP-labelled goat anti-human IgG (Jackson Immunoresearch) (1:3000) in casein/0.05% DDM was added for 45 min. After five washes with TBS/0.05% Tween20, plates were developed by adding develop solution [1% 3,3′,5,5′-tetraethylbenzidine (Sigma-Aldrich), 0.01 % H_2O_2, 100 mM sodium acetate, 100 mM citric acid] and the reaction was stopped after 5 min by adding 0.8 M H_2SO_4. Absorbance was measured at 450 nm and data was visualized in GraphPad Prism.

For mutant E1E2 ELISA assays, plasmids expressing E1E2 or mutants were transfected in 293T cells, which were harevested and lysed after 72 h using TBS with 1% triton X-100. The lysates were diluted in TBS and loaded overnight at 4°C on 96-well half-area ELISA plates pre-coated with *Galanthus nivalis* lectin (Vector Laboratories). Plates were washed before incubating with serially diluted mAbs in casein blocking buffer for 90 min. After three washes with TBS, HRP-labelled goat anti-human IgG (1:3000 in casein block buffer) was incubated for 45 minutes. After five washes with TBS/0.05% Tween20, the plates were developed as described above.

Purification of E1E2 complexes

HEK293F cells were transfected at a density of ~1.5 x 10^6 cells/ml by mixing PEIMAX with plasmids containing full-length AMS0232 E1E2, StrepII-tagged AR4A HC Fab and AR4A LC in a 1:1.3:1.9 ratio. Cell pellets were harvested 72 h post transfection, washed with ice-cold PBS and solubilized in PBS containing 1% triton X-100 and cOmplete protease inhibitor cocktail tablets (Sigma Aldrich) (1.5 tablets/L of transfected cells). The lysate

was incubated at 4 °C for 30 min, centrifuged at 4,000g for 30 min, filtered and flowed over a Strep-Tactin XT 4Flow affinity resin. Resin was washed with twelve resin volumes of wash buffer 1 (0.1 M Tris-Cl, 0.15 M NaCl, 1 mM EDTA, 0.025% triton-X-100, pH 8) and sixteen resin volumes of wash buffer 2 (0.1 M Tris-Cl, 0.15 M NaCl, 1 mM EDTA, 0.1% *n*-dodecyl β-D-maltoside (DDM), pH 8). The complexes were eluted with buffer BXT supplemented with DDM (0.1 M Tris-Cl, 0.15 M NaCl, 1 mM EDTA, 50 mM biotin, 0.1% DDM, pH 8). The eluted proteins were concentrated in 100-kDa cutoff filters and then injected into a Superose 6 increase column equilibrated in TBS/0.1% DDM. Non-complexed strepII-tagged E1E2 was purified using the same procedure, except that AR4A HC Fab and AR4A LC plasmids were excluded from the transfection mix.

Sample preparation for negative stain EM

E1E2 glycoprotein complex in 0.1% DDM was diluted to 20 μg/ml with TBS and complexed with 3x molar excess of AR4A Fab. The sample was applied for 10 s to carbon-coated 400 mesh Cu grids, which had been glow discharged at 15 mA for 20 s (Solarus advanced plasma cleaning system, Gatan; Ar/O_2; 35 sccm; 50W). The complex was negatively stained with 2% (w/v) uranyl-formate for 50 s.

Negative stain data collection and image processing

Data was collected on a Tecnai Spirit electron microscope operating at 120 keV. Nominal magnification was 52,000 X with a pixel size at 2.06 Å at the specimen plane. The nominal defocus range was set between -1,500 and -2,000 nm and the electron dose was calibrated to 25 $e^-/Å^2$. FEI Eagle CCD (4k) camera was used to record micrographs. Leginon automated imaging interface was used for data acquisition (*61*).

The data was processed using cryoSPARC (*64*). Particles were selected from micrographs using blob picker. A total of 52,487 particles were extracted from micrographs. Approximately ~15,500 particles were selected using 2D classification for further processing in 3D. One round of Ab initio (n=2) and two rounds of heterogeneous refinement (n=2) produced the best 3D reconstruction of E1E2 glycoprotein in complex with

AR4A. The 3D reconstruction was further processed using non-uniform refinement and resulted in a map of ~20Å resolution.

Sample preparation for cryo-EM

Five plasmids were co-transfected (E1E2, AR4A heavy chain, AR4A light chain, AT1209 heavy chain and AT1209 light chain at a ratio of 1:1.2:1.5:1.7:2, respectively). Cell pellets were harvested 72 h post transfection, washed with ice-cold PBS and solubilized in PBS containing 1% triton-X-100 and cOmplete protease inhibitor cocktail tablets (Sigma Aldrich) (1.5 tablets/L of transfected cells). The lysate was incubated at 4 °C for 1 h, and clarified by centrifugation in a JLA 16.25 rotor at 39,500g for 1 h. The clarified lysate was flowed over Streptactin XT 4Flow, washed but before elution, the resin was first resuspended in 2ml of wash buffer two and 500x molar excess of peptidisc (peptidisc biotech) was added and incubated at 4 °C for 1 h. 100 mg of biobeads SM-2 (BioRad) were added to the resin containing the protein of interest and the peptidiscs and incubated O/N at 4 °C. Flowthrough containing excess of peptidisc excess was discarded and five resin volumes of elution buffer (0.1 M Tris-Cl, 0.15 M NaCl, 1 mM EDTA, 50 mM biotin, pH 8) were added to the resin. The protein was eluted slowly (6-24 h), then incubated with 5x molar excess of IGH505 Fab for 1 h at 4ºC. The complex was concentrated in a 30-kDa cutoff centrifugal filter unit and then injected into a Superose 6 increase column in TBS. Peak fractions corresponding to E1E2 in complex with AR4A, AT1209 and IGH505 Fabs were concentrated to 1mg ml^{-1}. Protein was measured by absorbance at 280 nm using 1 ABS = 1 mg ml^{-1}.

Next, UltrAuFoil R 1.2/1.3 300 mesh gold grids were plasma cleaned for 7 s using a Solarus advanced plasma cleaning system (Gatan) before loading the sample (Ar/O_2; 35 sccm; 50W). Subsequently, 3 µl of purified protein was loaded onto the grid and plunge-frozen into nitrogen-cooled liquid ethane using the Vitrobot mark IV (Thermo Fisher Scientific). The settings for the Vitrobot were as follows: Temperature: 4 °C, humidity: 100%, blotting time: 5 s with standard Vitrobot filter paper, Ø55/20mm, Grade 595, blotting force: 0 and wait time: 7 s.

Cryo-EM data collection

Grids were loaded into a Talos Arctica transmission electron microscope (Thermo Fischer Scientific) operating at 200kV and images acquired using a K2 Summit direct electron detector camera (Gatan). The data were collected at a total cumulative exposure of $50e^-/Å^2$, 9 s exposure time, 36 frames and 250 ms/frame (See Table 1 for more details). Magnification was set at 36,000x with a resulting pixel size of 1.15 Å/pix at the specimen plane. Automated data collection was performed using Leginon software (*61*). The data collection details are presented in Table S1.

Cryo-EM image processing

Image preprocessing was performed using the Appion image processing environment (*62*). Stacks of dose-fractionated image frames were aligned using the UCSF MotionCor2 software (*63*). Particles were selected from the drift-corrected images (initial dataset, 2,650 images; second dataset, 2,471 images; for a total of 5,121 micrographs) using the cryoSPARC image processing suite (*64*). We estimated the CTF using GCTF (*65*) and extracted our particles at 1.15 Å/pixel with a box size of 300 x 300 pixels. A total of 2,017,845 particles were extracted from micrographs and 2D classified. A total of 1,049,598 particles were selected based on signal to noise ratio for further processing in 3D. Two rounds of heterogeneous classification (n=2 and n=4, respectively, with default parameters) produced one 3D class containing 34% of the particles that represented E1E2 in complex with three Fabs (AT1209 Fab, AR4A Fab and IGH505 Fab). Additionally, two classes containing 42% of the particles resembled E1E2 in complex with two Fabs (IGH505 Fab and AR4A Fab) (Supplementary Fig. 2C). In total, 355,643 particles from the representative class that we hypothesized contained E1E2 in complex with three Fabs was selected for non-uniform refinement, which generated a model with a reported a resolution at 3.49 Å based on a Fourier Shell Correlation (FSC) cutoff at 0.143. The 3.49 Å E1E2 reconstruction was further analyzed using 3D variability analysis (3DVA) using 3 eigenvectors and 8 clusters. Two clusters were selected based on visible secondary structural elements in E1 as well as a more defined peptidisc region. To ensure the density in

this region was due to signal from E1 and not noise, the 48,546 particles from these two clusters were used for 3D non-uniform refinement. The resulting model resolved to 3.83Å and provided additional insight into the structure of E1, particularly its membrane associated helices. We masked the flexible regions of E1 (highlighted in Supplemental Fig. 2D) for local refinement using all 1,049,598 particles. Local refinement generated a 3.37 Å map that enabled us to resolve additional, highly flexible regions of E1.

Model building and refinement

Two postprocessed maps were used to build the final atomic models. The first map contains E1, E2 and the 3 Fabs. Phenix map-to-model option was used to build E1 and E2 into the model (*66*). Two fragments of 15 amino acids were chosen to start de novo building in both models. Precise sequence registry assignment was determined by locating bulky Phe, Arg, Tyr, and Trp side chains. Iterative manual model building and automatic refinement were carried out in Coot. ABodyBuilder was used to produce the models of both antibody Fv regions (*67*). Multiple rounds of Rosetta relaxed refinement (*68*) and manual Coot refinement were performed to build the final models. Model fit to map was validated using MolProbity (*69*) and EMRinger (*70*) analyses. The final refined models were validated using Phenix 1.17.1 and submitted to the Protein Data Bank (PDB). All structural figures were generated using UCSF ChimeraX (*71*).

AlphaFold Prediction Software

AlphaFold *(72)* was used as a prediction software to determine the atomic model for both E1 and E2 individually. Specifically, the jupyter notebook module of ColabFold (AlphaFold2_advanced.ipynb) was utilized and accessed from the following link:

https://colab.research.google.com/github/sokrypton/ColabFold/blob/main/beta/AlphaFold2_advanced.ipynb#scrollTo=pc5-mbsX9PZC

The run parameters were as followed: (1) sequence (for E1 and E2, respectively): "YQVRNSTGLYHVTNDCPNSSIVYETADAILHTPGCVPCVREGNASRCWVPMTPTVATRDGKLPATQL RRHIDLLVGSATLCSALYVGDLCGSVFLVGQLFTFSPRRHWTTQDCNCSIYPGHVTGHRMAWDMMM NWSPTTALVVAQLLRIPQAILDMIAGAHWGVLAGLAYFSMVGNWAKVLAVLLLFAGVDA", "QTYVTGGTAARATSGLANFFSPGAKQDVQLINTNGSWHINRTALNCNTSLETGWIAGLIYLNKFNSSG CPERMASCRPLADFAQGWGPISYANGSGPDHRPYCWHYPPKPCGIVSAKSVCGPVYCFTPSPVVVGTT NKLGAPTYSWGENETDVFVLNNTRPPLGNWFGCTWMNSTGFTKVCGAPPCAIGGVGNNTLHCPTDCF RKHPEATYSRCGSGPWITPRCLVDYPYRLWHYPCTINYTRFKVRMYIGGVEHRLDAACNWTRGERCD LEDRDRSELSPLLLSTTQWQVLPCSFTTLPALSTGLIHLHQNIVDVQYLYGVGSSIVSWAIKWEYVVLLF LLLADARVCSCLWMMLLISQAEA" (2) jobname: "E1" or "E2" and (3) homooligomer: 1.

Site-specific glycan analysis

Two aliquots of the purified E1E2+AR4A+AT1209 Fab or E1E2 alone were denatured for 1h in 50 mM Tris/HCl, pH 8.0 containing 6 M of urea and 5 mM dithiothreitol (DTT). Next, the sample was reduced and alkylated by adding 20 mM iodoacetamide (IAA) and incubated for 1h in the dark, followed by a 1h incubation with 20 mM DTT to eliminate residual IAA. The alkylated E1E2 proteins were buffer-exchanged into 50 mM Tris/HCl, pH 8.0 using Vivaspin columns (3 kDa) and two of the aliquots were digested separately overnight using chymotrypsin (Mass Spectrometry Grade, Promega) or alpha lytic protease (Sigma Aldrich) at a ratio of 1:30 (w/w). The next day, the peptides were dried and extracted using C18 Zip-tip (MerckMilipore). The peptides were dried again, re-suspended in 0.1% formic acid and analyzed by nanoLC-ESI MS with an Ultimate 3000 HPLC (Thermo Fisher Scientific) system coupled to an Orbitrap Eclipse mass spectrometer (Thermo Fisher Scientific) using stepped higher energy collision-induced dissociation (HCD) fragmentation. Peptides were separated using an EasySpray PepMap RSLC C18 column (75 µm × 75 cm). A trapping column (PepMap 100 C18 3µM, 75µM × 2cm) was used in line with the LC prior to separation with the analytical column. The LC conditions were as

follows: 280 min linear gradient consisting of 4-32% acetonitrile in 0.1% formic acid over 260 minutes followed by 20 min of alternating 76% acetonitrile in 0.1% formic acid and 4% ACN in 0.1% formic acid, used to ensure all the sample had eluted from the column. The flow rate was set to 300 nL/min. The spray voltage was set to 2.5 kV and the temperature of the heated capillary was set to 40 °C. The ion transfer tube temperature was set to 275 °C. The scan range was 375−1500 m/z. Stepped HCD collision energy was set to 15, 25 and 45% and the MS2 for each energy was combined. Precursor and fragment detection were performed using an Orbitrap at a resolution MS1= 120,000. MS2= 30,000. The AGC target for MS1 was set to standard and injection time set to auto which involves the system setting the two parameters to maximize sensitivity while maintaining cycle time. Full LC and MS methodology can be extracted from the appropriate Raw file using XCalibur FreeStyle software or upon request.

Glycopeptide fragmentation data were extracted from the raw file using Byos (Version 4.0; Protein Metrics Inc.). The glycopeptide fragmentation data were evaluated manually for each glycopeptide; the peptide was scored as true-positive when the correct b and y fragment ions were observed along with oxonium ions corresponding to the glycan identified. The MS data was searched using the Protein Metrics 305 N-glycan library with sulfated glycans added manually. To search for N-glycans at non-canonical motifs, the above library was instead added as a custom modification to search for glycans (common1) at any N. The relative amounts of each glycan at each site as well as the unoccupied proportion were determined by comparing the extracted chromatographic areas for different glycotypes with an identical peptide sequence. All charge states for a single glycopeptide were summed. The precursor mass tolerance was set at 4 ppm and 10 ppm for fragments. A 1% false discovery rate (FDR) was applied. The relative amounts of each glycan at each site as well as the unoccupied proportion were determined by comparing the extracted ion chromatographic areas for different glycopeptides with an identical peptide sequence.

Glycan compositions were grouped according to their level of processing. HexNAc(2)Hex(10–5) compositions were classified as oligomannose-type, HexNAc(3)Hex(5-6)/HexNac(3)Hex(5-6)Fuc were classified as hybrid, and remaining glycan compositions were classified as complex-type.

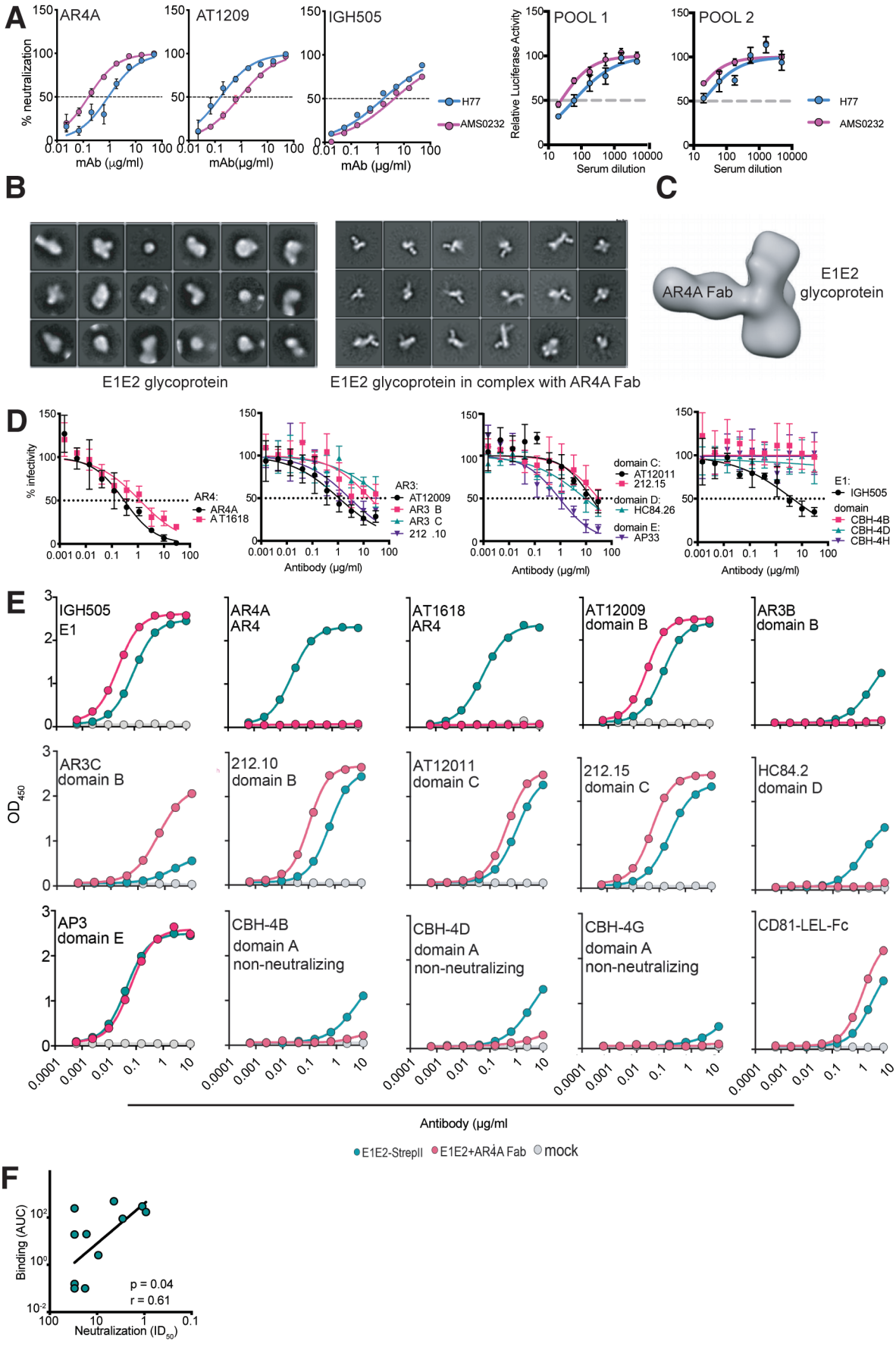
A
AR4A
AT1209
IGH505
% neutralization
mAb (μg/ml)
H77
AMS0232
POOL 1
POOL 2
Relative Luciferase Activity
Serum dilution
B
E1E2 glycoprotein
E1E2 glycoprotein in complex with AR4A Fab
C
AR4A Fab
E1E2
glycoprotein
D
% infectivity
AR4:
AR4A
AT1618
AR3:
AT12009
AR3 B
AR3 C
212 .10
Antibody (μg/ml)
domain C:
AT12011
212.15
domain D:
HC84.26
domain E:
AP33
E1:
IGH505
domain
CBH-4B
CBH-4D
CBH-4H
E
IGH505
E1
AR4A
AR4
AT1618
AR4
AT12009
domain B
AR3B
domain B
AR3C
domain B
212.10
domain B
AT12011
domain C
212.15
domain C
HC84.2
domain D
AP3
domain E
CBH-4B
domain A
non-neutralizing
CBH-4D
domain A
non-neutralizing
CBH-4G
domain A
non-neutralizing
CD81-LEL-Fc
OD450
Antibody (μg/ml)
E1E2-StrepII
E1E2+AR4A Fab
mock
F
Binding (AUC)
p = 0.04
r = 0.61
Neutralization (ID50)

Fig. S1. Biochemical characterization of AMS0232 pseudovirus and full-length recombinant AMS0232 E1E2 glycoprotein complex. (**A**) Pseudovirus neutralization experiments were performed in quadruplicates (n=4) for two pools of human sera and three monoclonal antibodies. Neutralization curves for bNAbs and serum pools to AMS0232 and H77 HCV pseudoviruses are plotted. (**B**) Negative-stain EM 2D class averages are shown for E1E2 and E1E2 in complex with AR4A Fab. (**C**) A 3D reconstruction of the negative-stain images of E1E2 in complex with AR4A is shown. (**D**) Neutralizing activity of monoclonal antibodies (tested in quadruplicate) against AMS0232 HCV pseudovirus. Error bars denote the S.D. Representative results from two independent experiments. (**E**) Binding of monoclonal antibodies and CD81 large extracellular loop (LEL) (Fc-tagged) to the purified E1E2 + AR4A Fab complex by enzyme-linked immunosorbent assay (ELISA). Representative results from two independent experiments. (**F**) Correlation between neutralization (ID_{50}) from *D* and antibody binding (area under the curve (AUC)) from *E.* Values for AR4A and AT1618 were left out for this analysis. Spearman r and p-values are indicated.

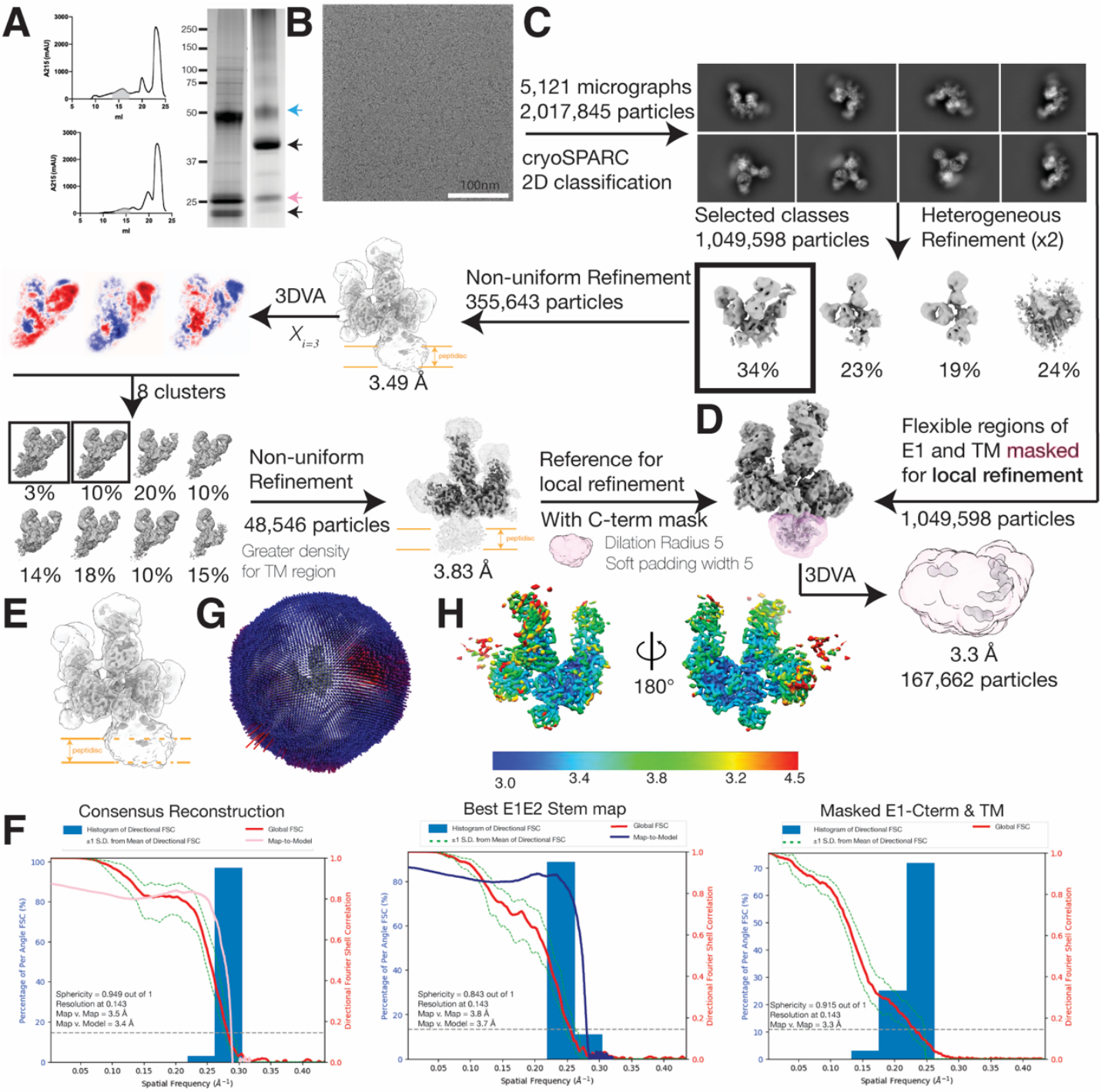

Fig. S2. CryoEM processing scheme of full-length HCV envelope glycoprotein E1E2 heterodimer in complex with bNAbs AT1209, IGH505 and AR4A. (**A**) Size-exclusion chromatography curves for full-length envelope glycoprotein E1E2 heterodimer in complex with bNAbs AR4A and AT1209 embedded in a DDM micelle (top panel) and full-length envelope glycoprotein E1E2 heterodimer in complex with bNAbs AT1209, IGH505 and AR4A embedded in a peptidisc (bottom panel) are shown. The area corresponding to E1E2-bNAb complexes are highlighted in light gray. SDS-PAGE gels of E1E2 in complex with Fabs under reducing (left lane) and non-reducing (right lane) conditions, respectively. The blue arrow at 50 kDa represents E2, the pink arrow at 25 kDa represents E1, and the black arrows represent the Fabs. (**B**) Raw micrograph of full-length HCV envelope glycoprotein E1E2 heterodimer in complex with bNAbs AT1209, IGH505, and AR4A collected on the Talos

Arctica with a pixel size of 1.15 Å/pixel. (**C**) A total of 2,017,845 particles were extracted from micrographs and 2D/3Dclassified using the cryoSPARC image processing suite(*57*). Next, 355,643 particles from the representative class that we hypothesized contained E1E2 in complex with three Fabs was selected for non-uniform refinement, which generated a model with a reported a resolution at 3.49Å. The final model resolved to 3.83Å and provided additional insight into the structure of E1, particularly its stem region. (**D**) Local refinement was performed to extract valuable signal from the stem and TMDs of E1E2. Using 1,049,598 particles from panel C, we ran multiple rounds of 3DVA and local refinement with the mask highlighted in pink to generate a 3.3 Å map of the E1 stem. The respective FSC curve of the local resolution map is to the right. (**E**) Overlay of the unsharpened 3.83 Å E1E2 map with threshold of 0.3 in ChimeraX with the sharpened 3.83 Å E1E2 map at a higher threshold of 0.1 in ChimeraX and the local resolution map to showcase the relative position of E1E2 to the membrane. (**F**) Three-Dimensional Fourier Shell Correlation (3DFSC) plot of the three maps. The $FSC_{map\text{-}map}$ resolution is calculated using 0.143 as the gold standard criterion, which represents how well the two half-maps from each dataset correlate as a function of spatial frequency. The $FSC_{map\text{-}model}$ curve, calculated in Phenix at a threshold of 0.143, was scaled proportionately and overlayed onto the following maps: (i) the consensus reconstruction and (ii) the Best E1E2 Stem map. (**G**) Angular distribution of the E1E2 maps. (**H**) Local resolution estimation for the consensus refinement. For data collection parameters and details, please reference Table S1.

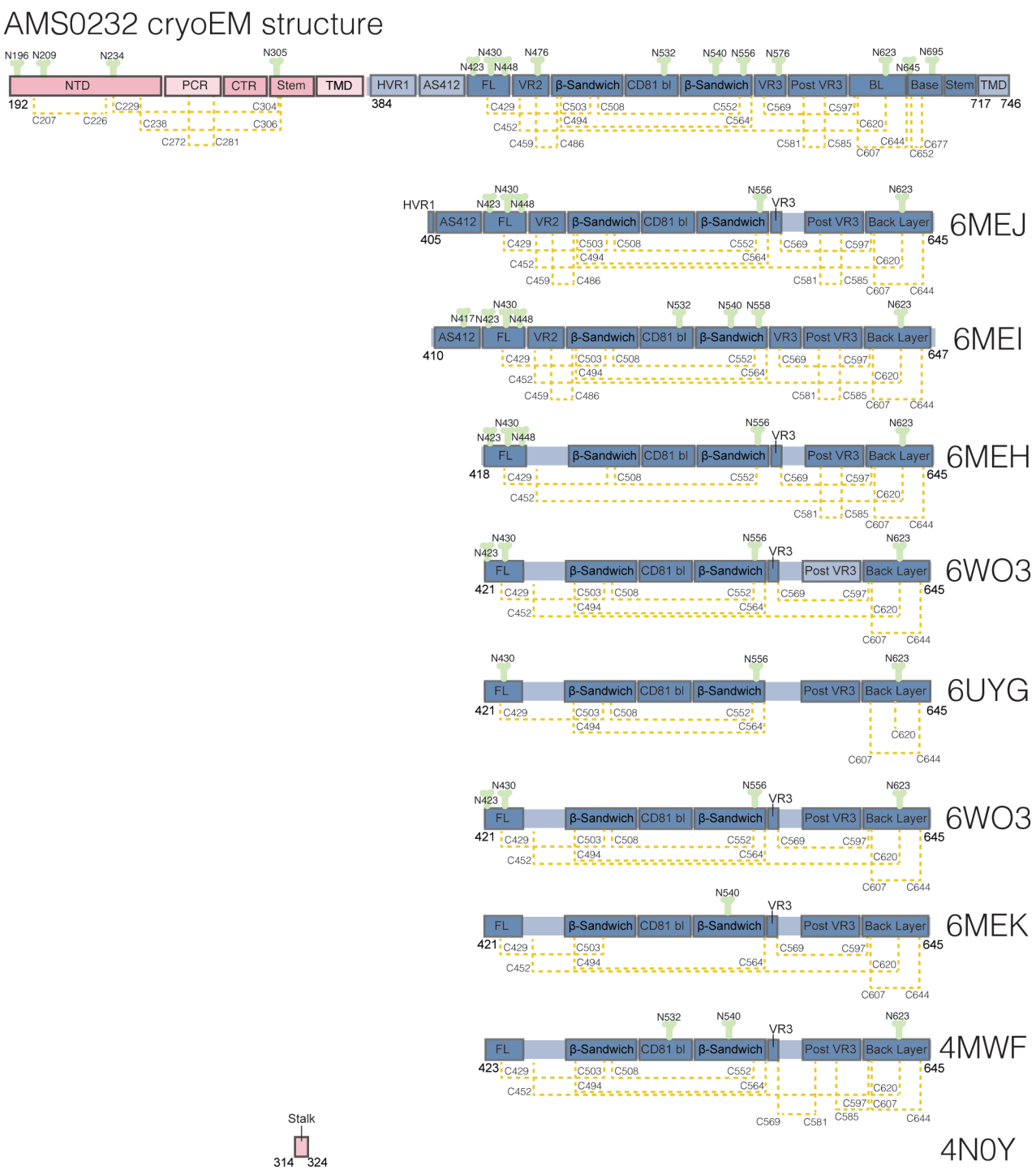

Fig. S3. Schematic representation of the regions resolved in our AMS0232 CryoEM structure compared to previous crystal structures of E1 and E2. The solved regions are highlighted in dark pink and dark blue for E1 and E2, respectively. The unresolved regions are depicted in light pink and light blue. N-linked glycans are shown in green and numbered with their respective Asn residues. Disulfide bonds are shown in yellow dashed lines and numbered accordingly. PDB IDs from previous crystal structures are indicated.

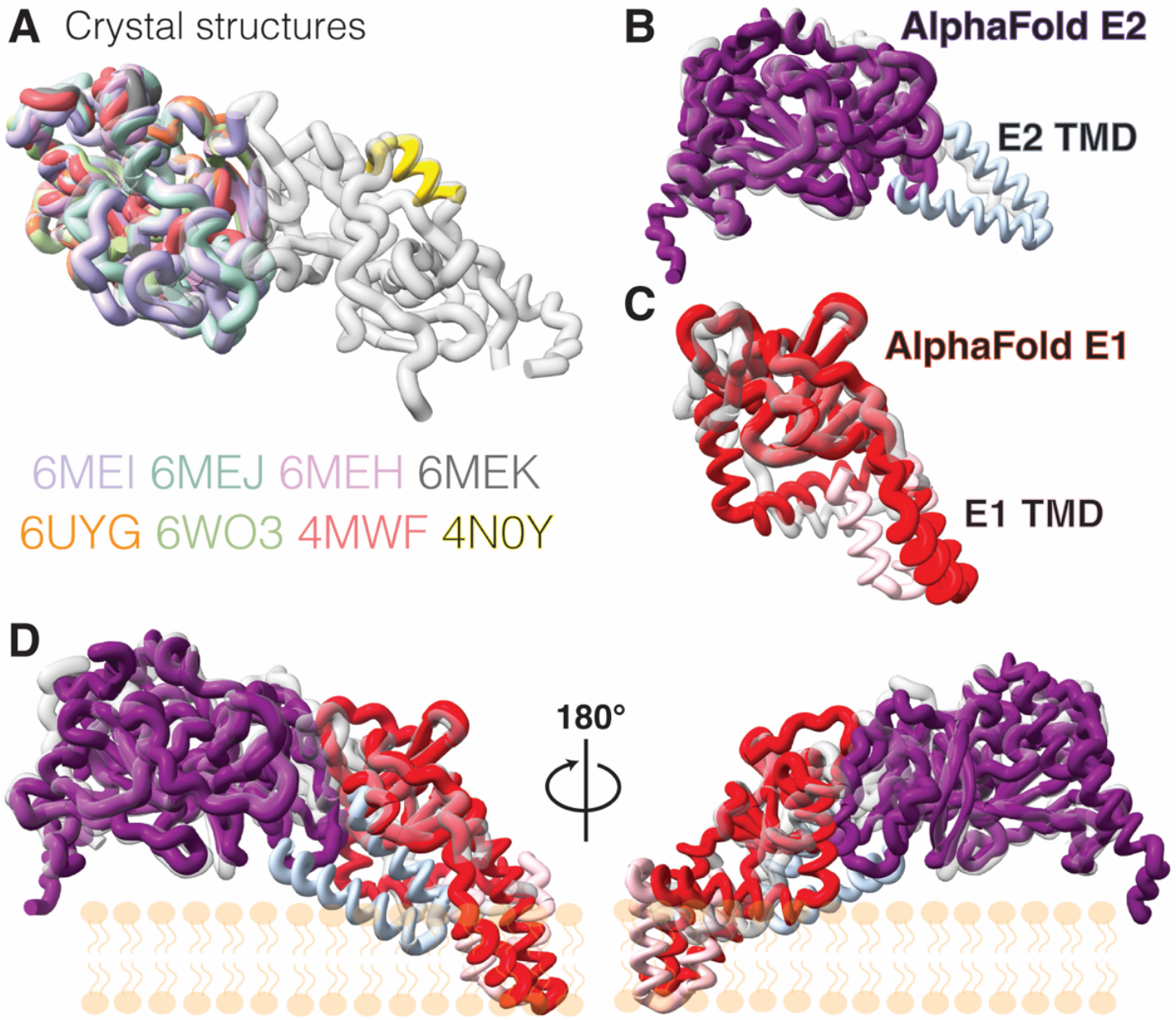

Fig. S4. Overlay of cryoEM full-length HCV E1E2 with published complementary crystal structures and the corresponding AlphaFold predictions. (**A**) The following crystal structures of individual segments of E1 or E2 are superimposed to highlight the novel regions of E1E2 discovered by our cryoEM structure: E2, 6MEI, 6MEJ, 6MEH, 6MEK, 6UYG, 6WO3, 4MWF; E1, 4N0Y. Our cryoEM structure is transparent here for adequate comparison and further compared with the corresponding AlphaFold structures for (**B**) E2; in purple, with its TMD highlighted in light steel blue; and (**C**) E1; in red, with its TMD highlighted in pink. (**D**) Full-length E1E2 cryoEM structure (atomic model; spaghetti cartoon) superimposed with the AlphaFold E1 and E2 models. A lipid bilayer schematic represented in orange is shown to orient E1E2 heterodimer atomic model and the AlphaFold predicted model relative to the viral membrane.

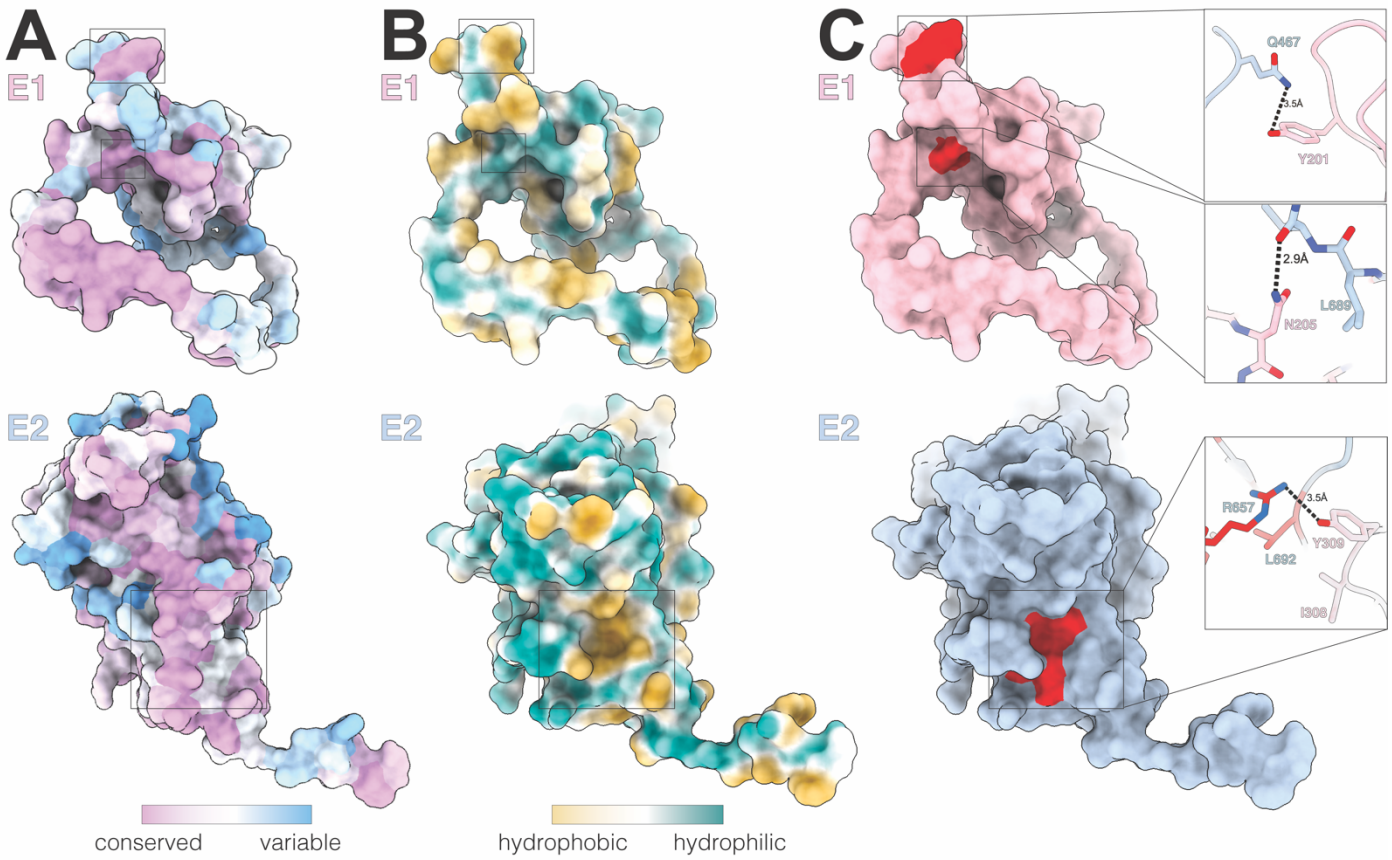

Fig. S5. Conservation and mutational analysis (Pfaff-Kilgore et al. Cell Rep 2022) of the E1E2 interface reveal amino acids that are critical for E1E2 assembly. (**A**) Conservation plot of E1 and E2 (conserved = purple; non-conserved = blue; see key). N-linked glycans were left out of the comparison. (**B**) Hydrophobic schematic of the E1 and E2 interface (hydrophobic = yellow; hydrophilic = blue; see key). (**C**) Key residues (red) that participate in significant interactions at the interface. For E1: Y201 forms a salt bridge with Q467 and N205 can form a salt bridge with the amino acid backbone, as shown in small panels to the right. Y201 is hydrophobic and highly conserved, while N205 is primarily conserved. The E2 domain is colored in light steel blue and mutants which were shown to be critical for E1E2 assembly according to the mutational analysis study (Pfaff-Kilgore et al. Cell Rep. 2022) are colored in red. Residues R657, D658, F679, L692, buttress the hydrophobic cavity of E2, a feature essential for the E1E2 interface, however, only R657 and L692 make significant contacts with E1, a salt bridge with Y309, and hydrophobic contacts with I308 and Y309 (within a 4 Å distance), respectively.

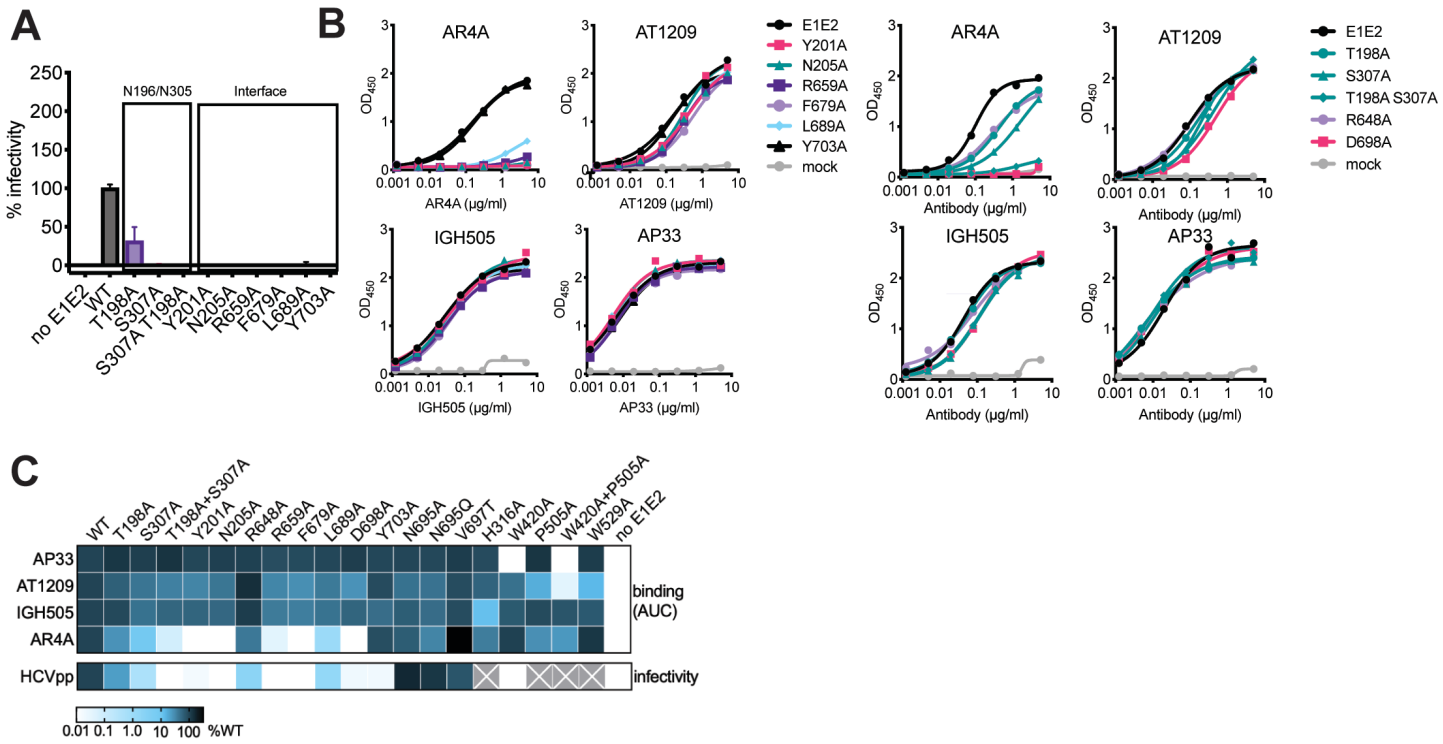

Fig. S6. Summary of the E1E2 interface mutants and their effects on HCV infectivity and antigenicity. (**A**) Infectivity of E1E2 interface mutants measured in an HCV pseudoparticle assay. Mutagenesis of the E1E2 interface result in a loss of infectivity for HCV pseudoparticles. Error bars denote standard deviation (S.D.). Experiments were done in replicates of five and were performed two to three times and values were normalized to wild-type (WT) AMS0232 E1E2. (**B**) Binding of AR4A, AT1209, IGH505 and AP33 (loading control) antibodies to mutant E1E2 glycoproteins, produced in HEK293T as cell lysates, is shown. Representative results are from two independent experiments. (**C**) Heat map summarizing the results of E1E2 mutants (figs. S6A, S8A, and S11). The binding was calculated as mean of the area under the curve (AUC) from two independent experiments (representative curves are shown in figs. S6B, S8B, and S11B) and the percentage of infectivity and binding was normalized to 100% for WT E1E2. Gray boxes represent data that is not available.

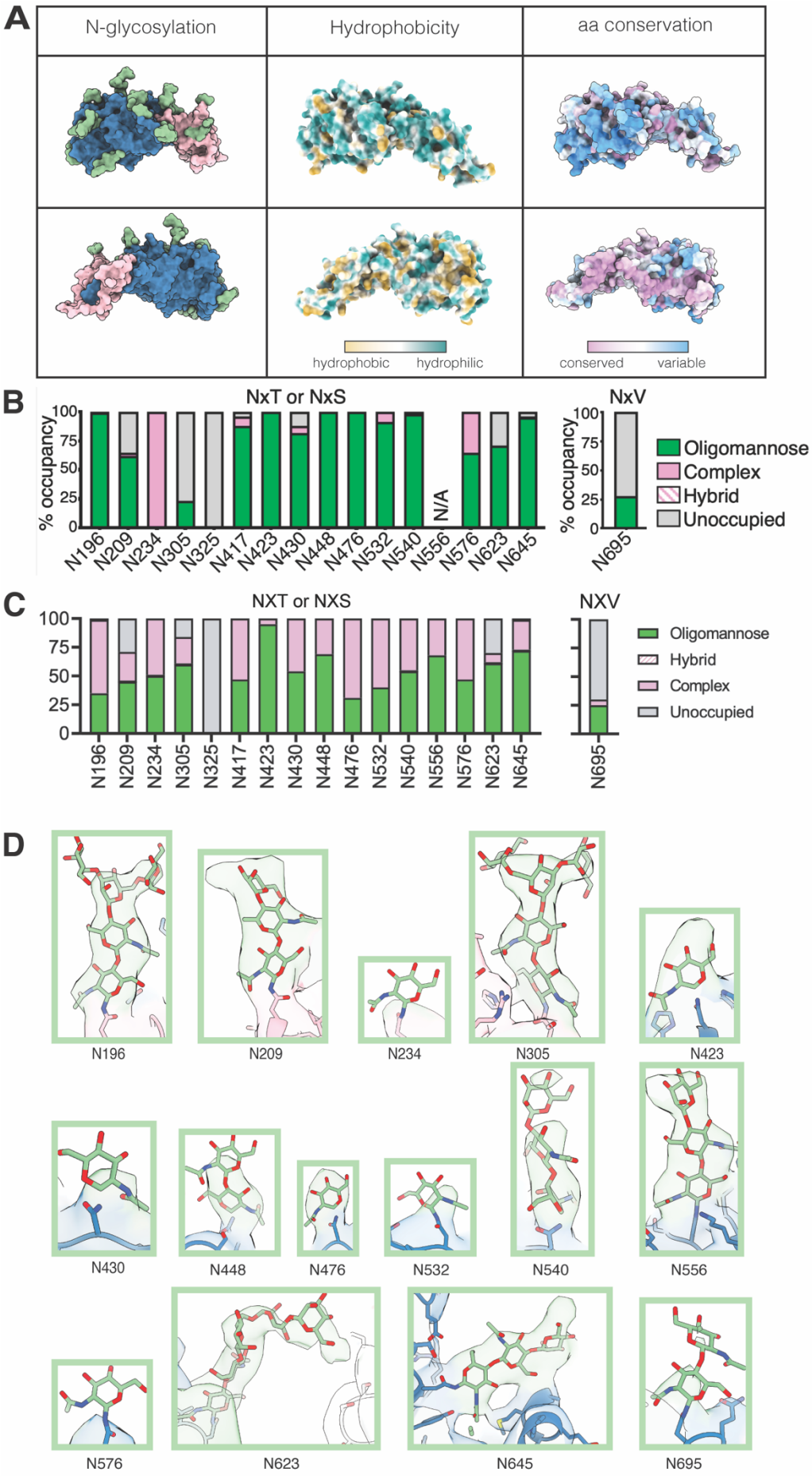
A
N-glycosylation
Hydrophobicity
aa conservation
hydrophobic
hydrophilic
conserved
variable
B
NxT or NxS
NxV
% occupancy
100
75
50
25
0
N196
N209
N234
N305
N325
N417
N423
N430
N448
N476
N532
N540
N556
N576
N623
N645
N/A
N695
Oligomannose
Complex
Hybrid
Unoccupied
C
NXT or NXS
NXV
Oligomannose
Hybrid
Complex
Unoccupied
D
N196
N209
N234
N305
N423
N430
N448
N476
N532
N540
N556
N576
N623
N645
N695

Fig. S7. **Glycosylation analysis of E1E2 glycoprotein complex**. (**A**) N-glycosylation sites (in green) on the surface of E1 (pink) and E2 (blue) (left). Hydrophobicity of the surface exposed amino acids in E1 and E2 using the Kyte-Doolittle hydrophobicity scale (middle). Sequence conservation of surface exposed amino acids of E1E2 (right). Top row is 180^{o} rotated compared to the bottom row. Relative quantification of distinct glycan types of full-length AMS0232 E1E2 bound to three Fabs (**B**) and unbound full-length E1E2 (**C**) glycoprotein complex determined by LC-MS. The bar graphs show the relative percentage of the glycan processing state at a particular site. Oligomannose-type glycans are shown in green, hybrid in dashed pink, complex glycans in pink and unoccupied sites in gray. N/A, data not available. (**D**) Glycans densities (green) are shown at threshold of 0.19 in ChimeraX. The unsharpened non-focused map of the full complex that produced the best density for E2 stem residues 708-717, as labeled in the PDB deposition, or Best E1E2 Stem map, in Extended Data Fig. 2, was used to generate this visualization. We observed N576 is visible at low signal-to-noise thresholds, while N325 is not. N417 resides in the AS412 region, which remains unresolved in our structure. E1 is shown in pink and E2 is shown in steel blue.

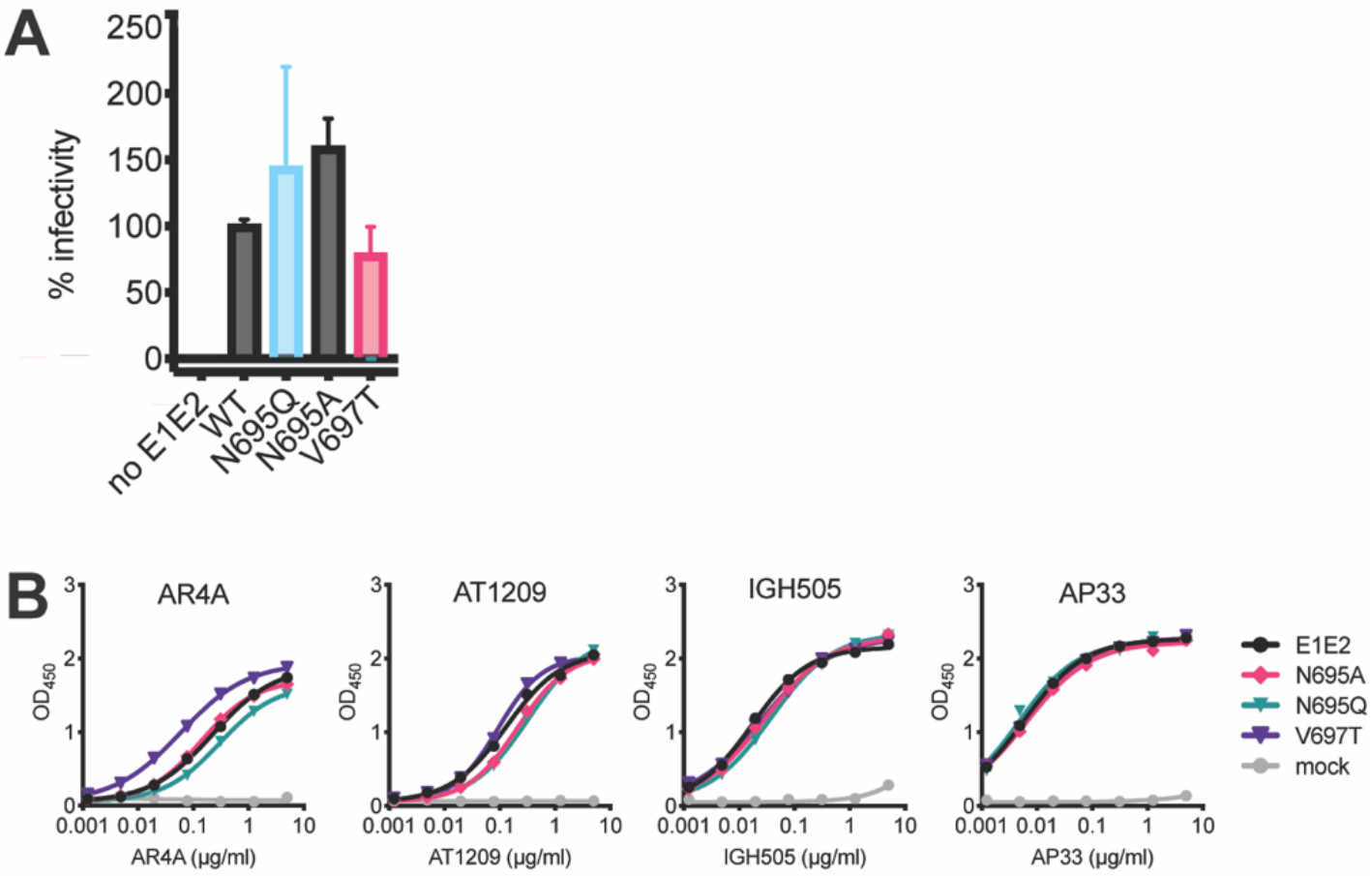

Fig. S8. Summary of the NxV glycan site mutants and their effects on HCV infectivity. (**A**) Infectivity of E1E2 mutants in HCV pseudoparticles. Error bars denote standard deviation (S.D.) Experiments were done in replicates of five and were performed two to three times. (**B**) E1E2 glycoproteins from HEK 293T lysates were tested for binding to monoclonal antibodies. Representative results are from two independent experiments.

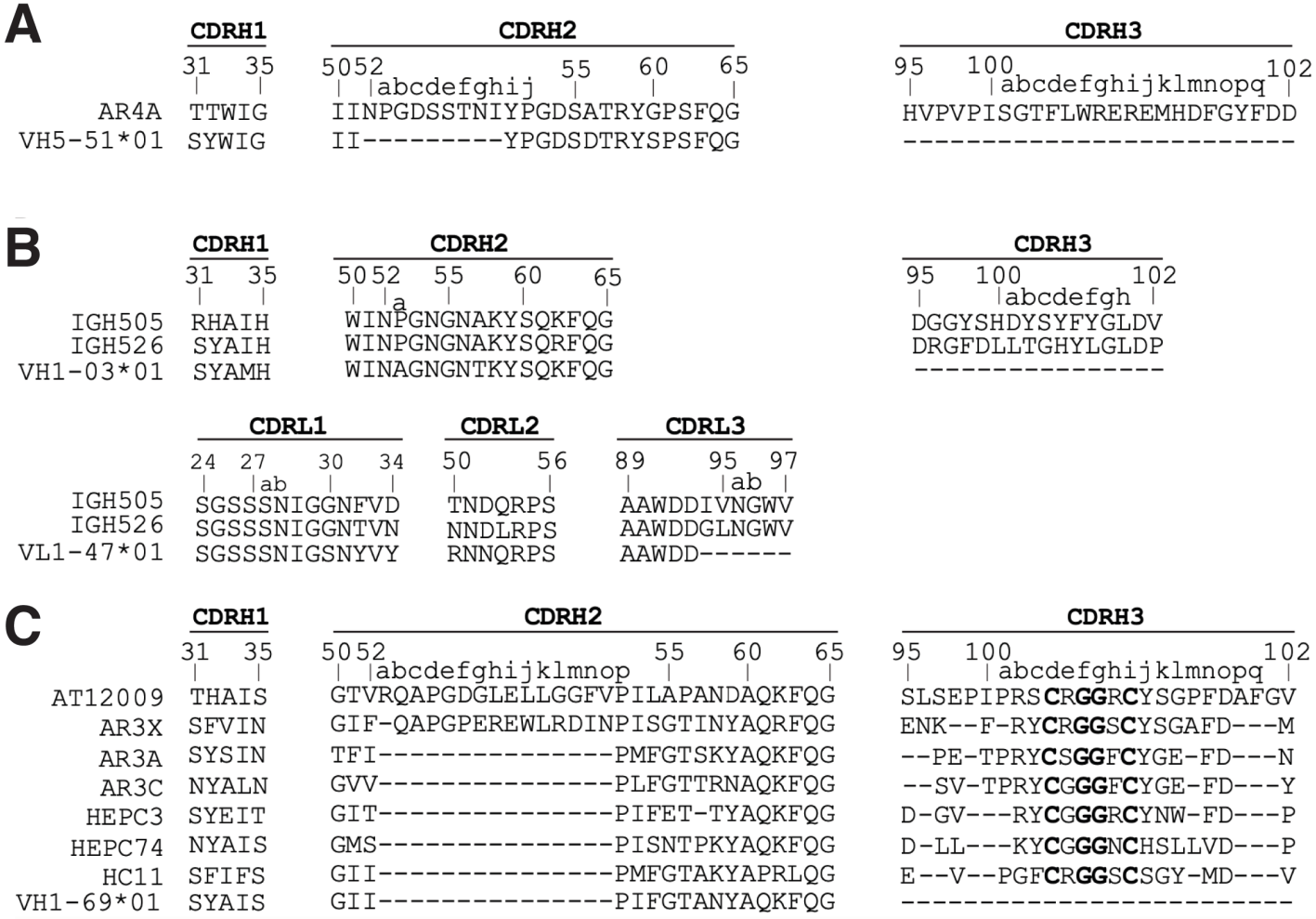

Fig. S9. Alignment of the bNAbs AR4A, AT1209 and IGH505 to their inferred germline. (**A**) Alignment of the CDRH1-3 of AR4A with its inferred VH5-51*01 germline gene. (**B**) Alignment of the CDRH1-3 and CDRL1-3 of IGH505 and IGH526 with their respective inferred germline genes. (**C**) Alignment of the CDRH1-3 of AT1209 with related AR3-targeting bNAbs that harbor the CxGGxC motif in their CDRH3 and VH1-69*01. CDR annotation and antibody numbering according to Kabat.

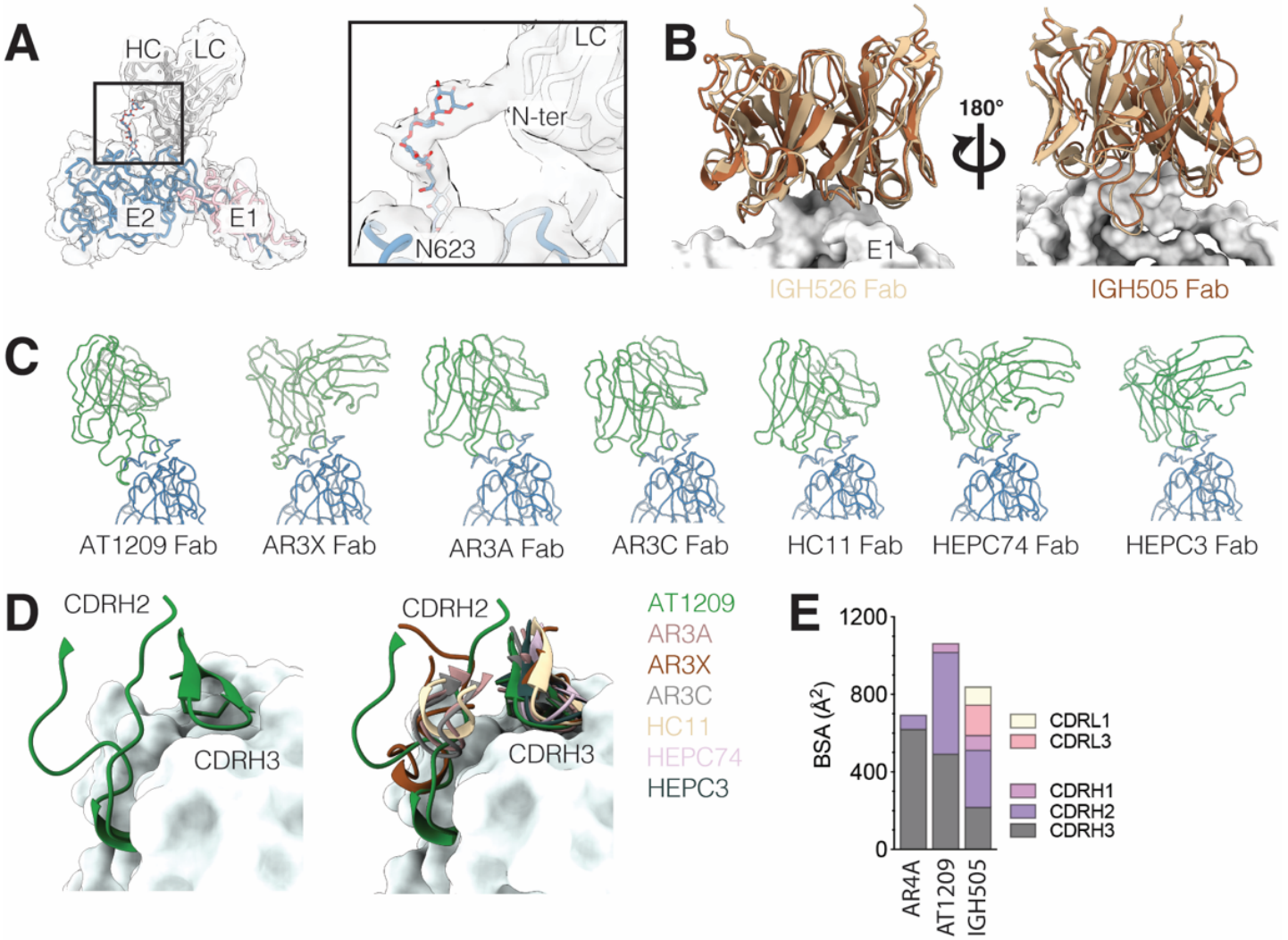

Fig. S10. AT1209 and IGH505 share epitopes with previously known HCV bNAb antibodies. (**A**) While AT1209 and IGH505 only interact with E2 and E1 peptide region respectively, AR4A Fab not only interacts with the E2 peptide (Fig. 4b) but also with the glycan N623. The unsharpened map is shown in white with the N623 glycan moieties shown in blue and colored by heteroatom interacting with the N-ter domain of the light chain. (**B**) The IGH505 Fab targets the same epitope as IGH526 (PDB 4N0Y) and adopts the same angle of approach. The IGH505 and IGH526 bNAbs are overlayed and shown in brown and yellow respectively. (**C**) CDRH3 motif in E2 front layer-specific HCV bNAbs adopt different orientations. Fab structures in liganded state of AT1209, AR3X (PDB 6URH), AR3A (PDB 6UYM), AR3C (PDB 6UYD), HC11 (PDB 6W04), HEPC74 (PDB 6MEH) and HEPC3 (PDB 6MEJ) are shown. The structures were superimposed on their E2 subunit. Protein backbones are colored green for Fabs and blue for E2 and shown as ribbons. (**D**) The AT1209 ultralong CDRH2 and CDRH3 loops are shown in green laying on the front layer of E2. CDRH2-3 of all HCV bNAb antibodies that target the front layer of E2 are superimposed and shown in different colors. (**E**) Buried surface area between E1E2 and the CDR loops of the AR4A, IGH505 and AT1209 bNAbs.

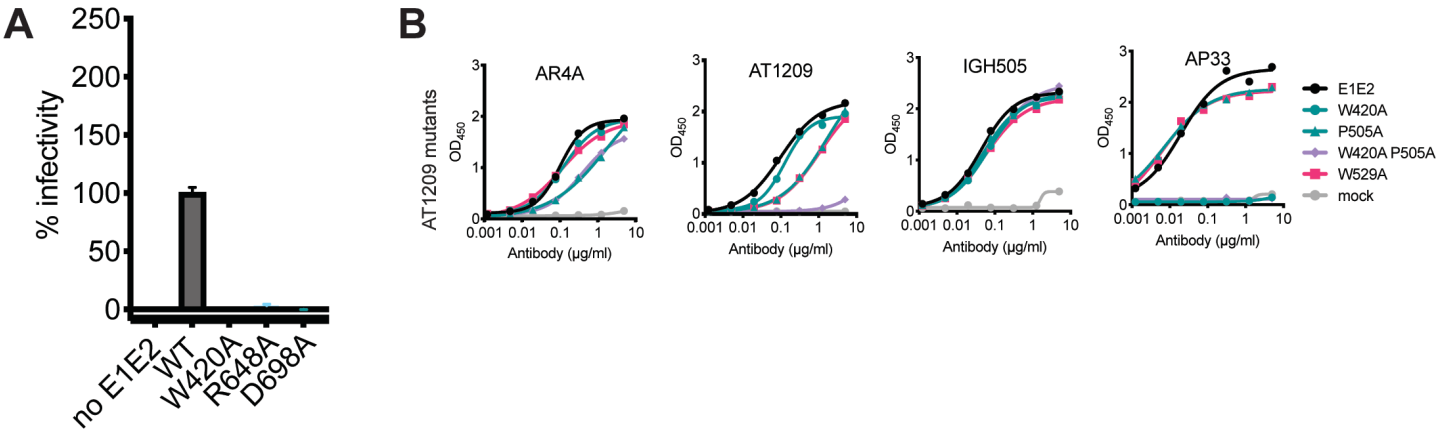

Fig. S11. Summary of the AR4A and AT1209 epitope mutants and their effects on HCV infectivity and antigenicity. (**A**) Infectivity of E1E2 mutants (W420A, R648A and D698A) from HCV pseudoparticles is shown. Error bars denote S.D. from 5-plo of two to three experiments. (**B**) Antigenicity of E1E2 mutants located at the AT1209 epitope was tested by using HEK 293T lysates and assessing its binding of monoclonal antibodies. Representative results are from two independent experiments.

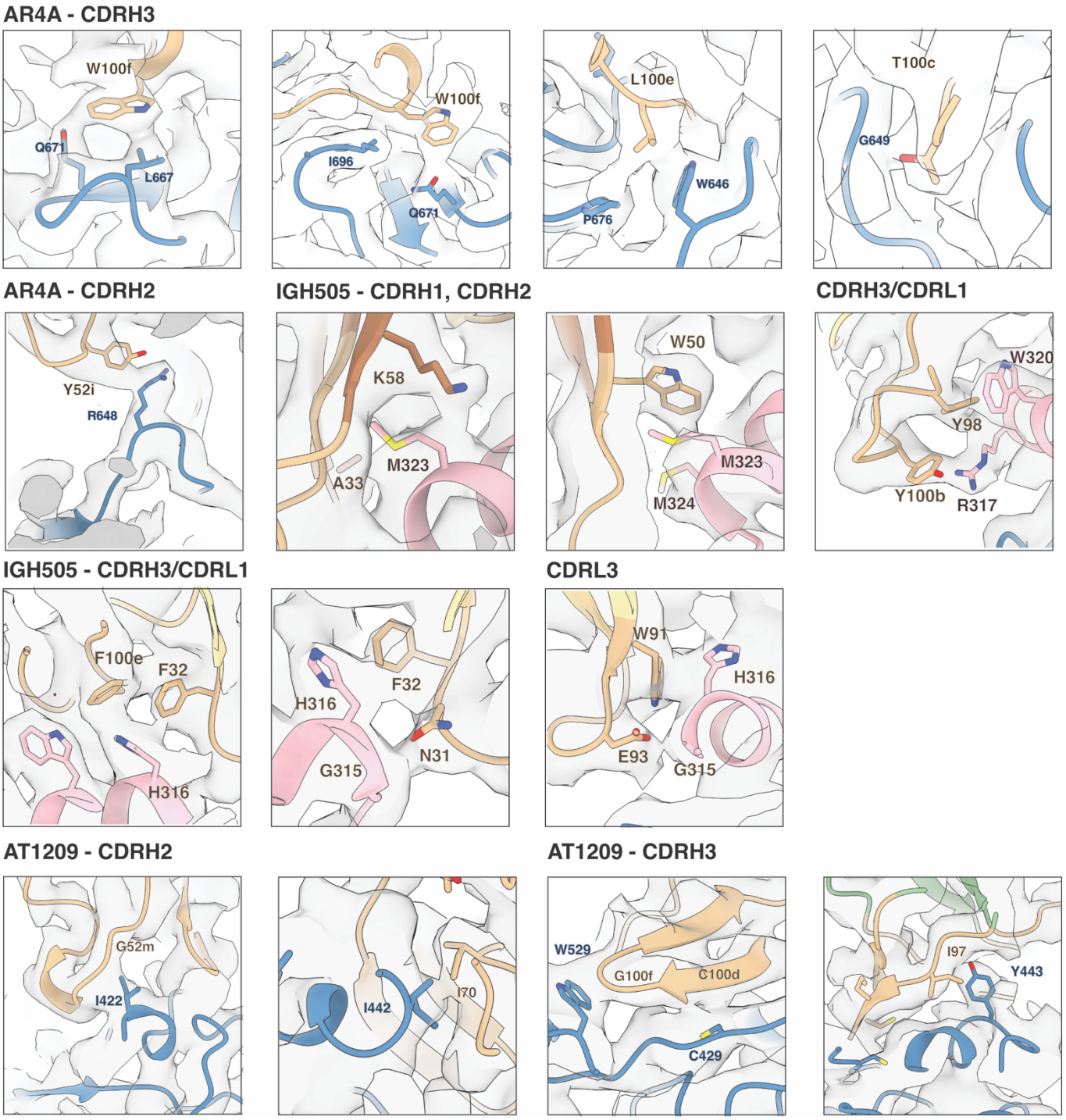

Fig. S12. Close-up views of the amino acid residues involved in the epitope/paratope between E1E2 glycoprotein complex and AR4A, AT1209 and IGH505 Fabs. Models (ribbon representation) and maps (light gray) are shown and close-up views of each structure with the most relevant epitope/paratope amino acids are indicated. Contact densities are shown at a threshold of 0.1 in ChimeraX.

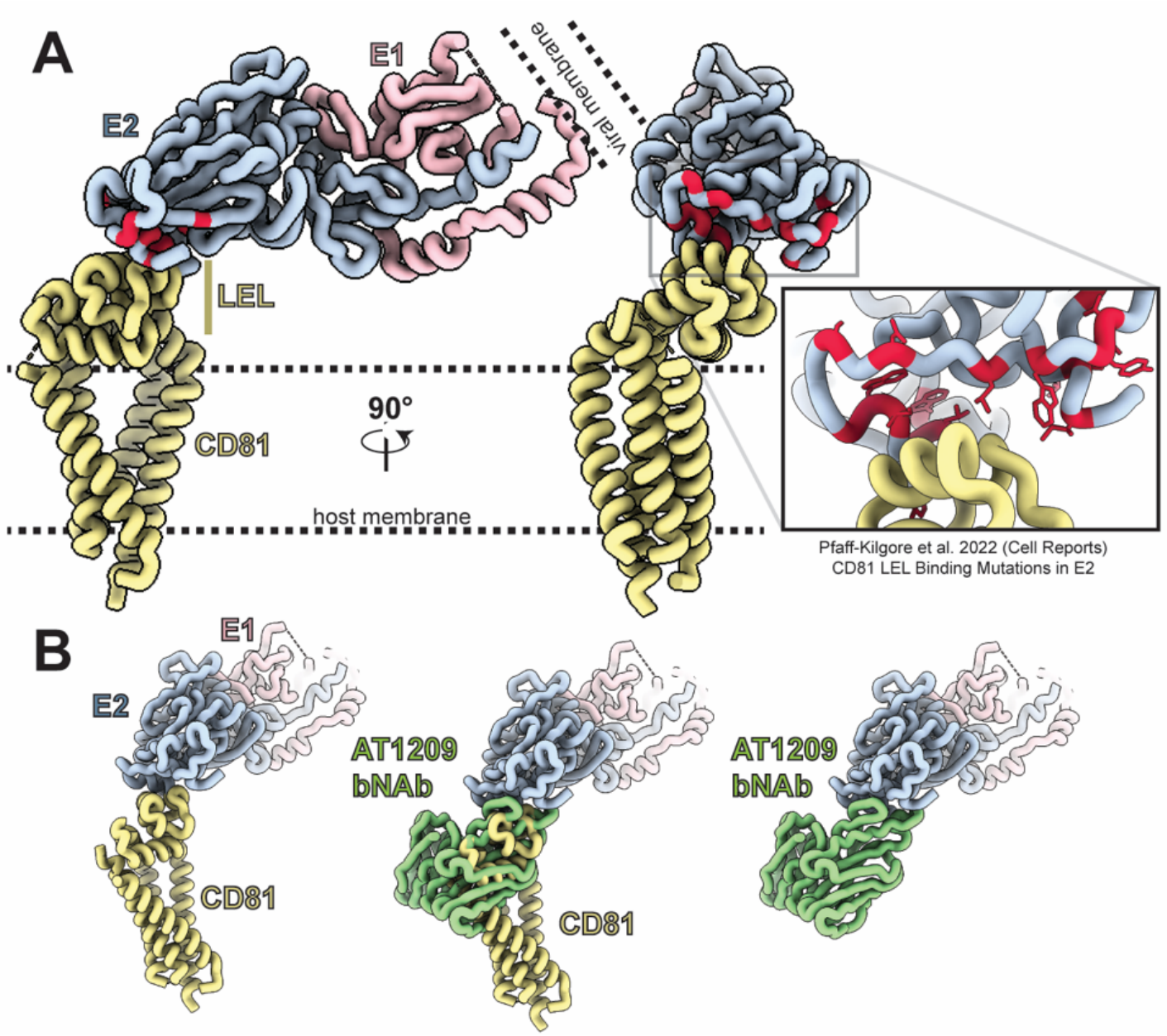

Fig. S13. Mutational analysis reveals amino acids that are critical for host receptor CD81 engagement by E2. (**A**) Full-length E1E2 atomic model generated in our study docked on the full-length CD81 structure (PDB: 5TCX) with amino acids that are important for CD81-LEL binding according to Pfaff-Kilgore et al. colored in red (I422, S424, L427, N430, S432, G436, W437, L438, G440, L441, F442, Y443, V515, T519, T526, Y527, W529, W616). The black dotted lines represent the host cell membrane to illustrate how CD81 is oriented and underscoring that the large cellular loop (LEL) of CD81 is exposed to engage E2 on the E1E2 complex. (**B**) Atomic model docking of CD81 and AT1209 reveals that AT1209 binding completely blocks E2 from interacting with CD81.

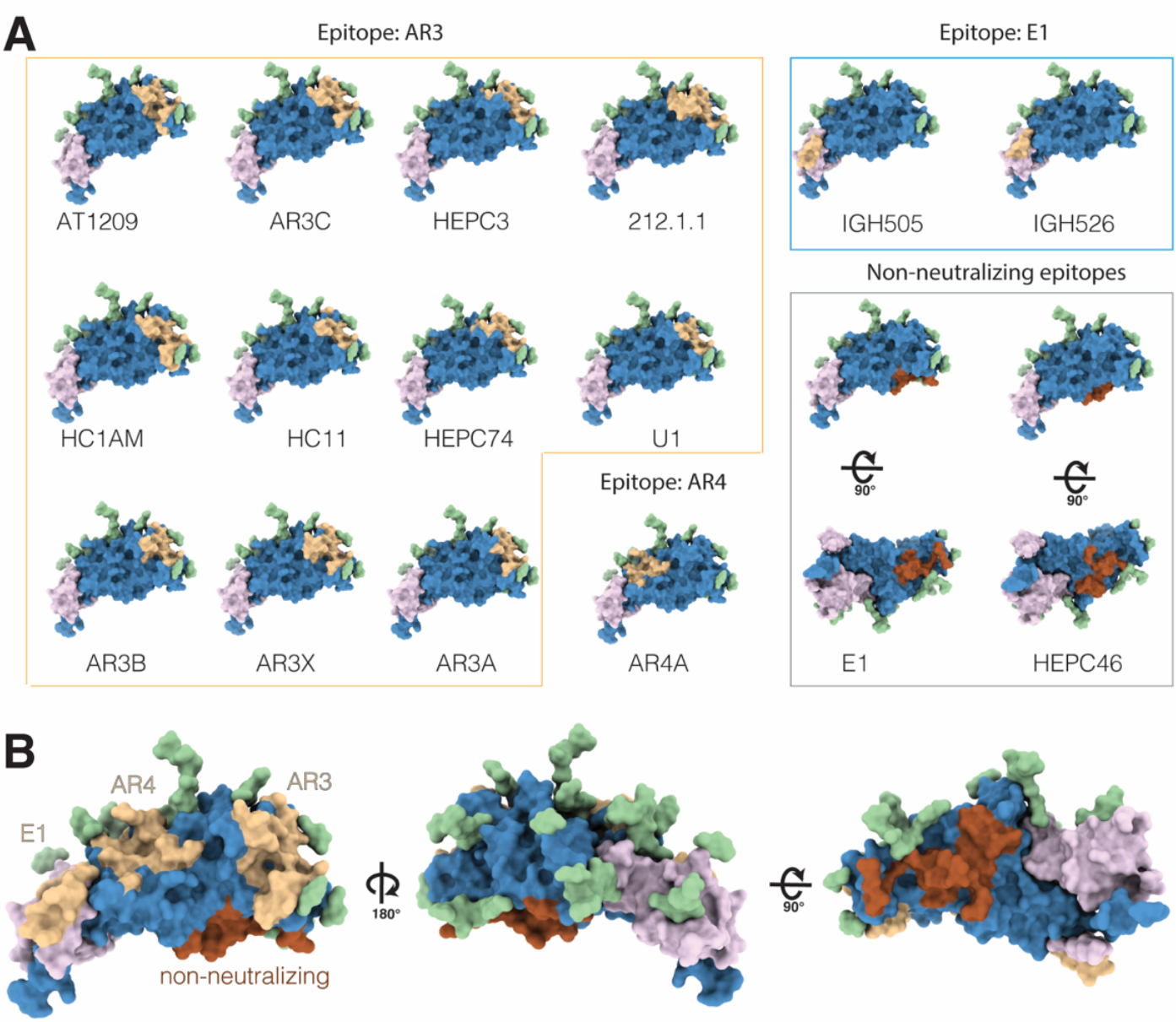

Fig. S14. Footprints of the epitopes of human NAbs and non-NAbs targeting E1E2 glycoprotein complex. **(A)** Comparison of antigenic region 3 (AR3) and antigenic region 4 (AR4) on E2, a neutralizing epitope on E1 and non-neutralizing epitopes. Footprints were defined on the E1E2 glycoprotein complex as atoms within 4 Å of the indicated Fab. Footprints of neutralizing antibodies are colored in wheat and non-neutralizing antibodies in brown. E2 is colored blue and E1 in pink. (**B**) Summary representation of the footprints of the NAbs and non-NAbs in a E1E2 glycoprotein complex defining a neutralizing face (left), glycan face (middle) and non-neutralizing face (right). For details about the buried surface area for each Fab, please see Table S2.

Table S1. **Data collection, image processing and map and model refinement parameters.**

	AMS0232-IGH505-AR4-AT1209 (EMDB 25730, PDB 7T6X)	C-terminal domain of E1-AMS0232
Data collection		
Microscope	Talos Arctica	
Voltage (keV)	200	
Detector	K2 Summit	
Magnification (nominal/calibrated)	36,000X/43,478X	
Exposure navigation *	Image shift 4/16 holes	
Data acquisition software	Leginon	
Total electron exposure (e-/Å^2)	50	
Exposure rate (e-/pixel/sec) *	6.074/6.754	
Frame length (ms)	250	
No. of frames per micrograph	49	
Pixel size (Å)	1.15	
Defocus range (μm)	-0.8 to -1.12	
Micrographs collected (no.)	5,121	
Reconstruction		
Image processing package	cryoSPARC	
Total extracted particles (no.)	1,049,598	
Refined particles (no.)	355,643	993,212
Final particles (no.)	48,546	167,662
Symmetry imposed	C1	C1
Resolution (Å)		
Map to Map		
FSC 0.5 (mask none / loose / tight)	8.1 / 4.9 / 4.2	6.8 / 5.2 / 4.3
FSC 0.143 (mask none / loose / tight)	4.6 / 4.1 / 3.8	4.8 / 3.8 / 3.7
Resolution range (local)	3.0 - 4.5	3.0 - 10.0
3DFSC Sphericity	0.949 out of 1	0.915 out of 1
Sharpening B-factor (Å^2)	-109	-117
Model Composition		
Protein residues	1,140	
Ligands	16	
N-acetyl-β-D-glucoseamine (NAG)	24	
α-D-mannose (MAN)	6	
β-D-mannose (BMA)	7	
Model Refinement and Validation		
Refinement and validation package	Rosetta, MolProbity and Phenix	
CC (volume / mask)	0.82 / 0.83	
R.m.s. deviations (Bond lengths / angles)	0.021 Å / 1.942º	
Map-to-model FSC (0.5)	3.9	
Ramachandran (%)		
Outliers / Allowed / Favored	0.09 / 3.83 / 96.08	
MolProbity score	1.33	
Poor rotamers (%)	0	
Clashscore (all atoms)	2.73	
C-beta deviations	0	
CaBLAM Outliers (%)	4.62	
EMRinger Score	2.79	

*These parameters include statistics that represent the following two datasets: 20nov20 and 21jul28.

Table S2. Buried surface area between E1E2 and the CDR loops of the AR4A, IGH505 and AT1209 bNAbs.

Antibody	Region	Interaction (subunit)	BSA (Å^2)*
AR4A	CDRH2	E2	72
	CDRH3	E2	622
IGH505	CDRH1	E1	76
	CDRH2	E1	295
	CDRH3	E1	219
	CDRL1	E1	93
	CDRL3	E1	122
	CDRL3	E2	35
AT1209	CDRH1	E2	45
	CDRH2	E2	493
	CDRH3	E2	526

* Buried Surface Area (BSA) was calculated using PDBePISA

References and Notes

1. T. R. Fuerst, B. G. Pierce, Z. Y. Keck, S. K. H. Foung, Designing a B cell-based vaccine against a highly variable hepatitis C virus. *Front. Microbiol.* **8**, 2692 (2018). doi:10.3389/fmicb.2017.02692 Medline

2. S. A. Yost, Y. Wang, J. Marcotrigiano, Hepatitis C virus envelope glycoproteins: A balancing act of order and disorder. *Front. Immunol.* **9**, 1917 (2018). doi:10.3389/fimmu.2018.01917 Medline

3. V. J. Kinchen, M. N. Zahid, A. I. Flyak, M. G. Soliman, G. H. Learn, S. Wang, E. Davidson, B. J. Doranz, S. C. Ray, A. L. Cox, J. E. Crowe Jr., P. J. Bjorkman, G. M. Shaw, J. R. Bailey, Broadly neutralizing antibody mediated clearance of human hepatitis C virus infection. *Cell Host Microbe* **24**, 717–730.e5 (2018). doi:10.1016/j.chom.2018.10.012 Medline

4. J. M. Pestka, M. B. Zeisel, E. Bläser, P. Schürmann, B. Bartosch, F.-L. Cosset, A. H. Patel, H. Meisel, J. Baumert, S. Viazov, K. Rispeter, H. E. Blum, M. Roggendorf, T. F. Baumert, Rapid induction of virus-neutralizing antibodies and viral clearance in a single-source outbreak of hepatitis C. *Proc. Natl. Acad. Sci. U.S.A.* **104**, 6025–6030 (2007). doi:10.1073/pnas.0607026104 Medline

5. S. J. Merat, C. Bru, D. van de Berg, R. Molenkamp, A. W. Tarr, S. Koekkoek, N. A. Kootstra, M. Prins, J. K. Ball, A. Q. Bakker, M. D. de Jong, H. Spits, T. Beaumont, J. Schinkel, Cross-genotype AR3-specific neutralizing antibodies confer long-term protection in injecting drug users after HCV clearance. *J. Hepatol.* **71**, 14–24 (2019). doi:10.1016/j.jhep.2019.02.013 Medline

6. M. Law, T. Maruyama, J. Lewis, E. Giang, A. W. Tarr, Z. Stamataki, P. Gastaminza, F. V. Chisari, I. M. Jones, R. I. Fox, J. K. Ball, J. A. McKeating, N. M. Kneteman, D. R. Burton, Broadly neutralizing antibodies protect against hepatitis C virus quasispecies challenge. *Nat. Med.* **14**, 25–27 (2008). doi:10.1038/nm1698 Medline

7. D. O'Shea, J. Law, A. Egli, D. Douglas, G. Lund, S. Forester, J. Lambert, M. Law, D. R. Burton, D. L. J. Tyrrell, M. Houghton, A. Humar, N. Kneteman, Prevention of hepatitis C virus infection using a broad cross-neutralizing monoclonal antibody (AR4A) and epigallocatechin gallate. *Liver Transpl.* **22**, 324–332 (2016). doi:10.1002/lt.24344 Medline

8. Y. P. de Jong, M. Dorner, M. C. Mommersteeg, J. W. Xiao, A. B. Balazs, J. B. Robbins, B. Y. Winer, S. Gerges, K. Vega, R. N. Labitt, B. M. Donovan, E. Giang, A. Krishnan, L. Chiriboga, M. R. Charlton, D. R. Burton, D. Baltimore, M. Law, C. M. Rice, A. Ploss, Broadly neutralizing antibodies abrogate established hepatitis C virus infection. *Sci. Transl. Med.* **6**, 254ra129 (2014). doi:10.1126/scitranslmed.3009512 Medline

9. B. D. Lindenbach, C. M. Rice, The ins and outs of hepatitis C virus entry and assembly. *Nat. Rev. Microbiol.* **11**, 688–700 (2013). doi:10.1038/nrmicro3098 Medline

10. P. Pileri, Y. Uematsu, S. Campagnoli, G. Galli, F. Falugi, R. Petracca, A. J. Weiner, M. Houghton, D. Rosa, G. Grandi, S. Abrignani, Binding of hepatitis C virus to CD81. *Science* **282**, 938–941 (1998). doi:10.1126/science.282.5390.938 Medline

11. E. Scarselli, H. Ansuini, R. Cerino, R. M. Roccasecca, S. Acali, G. Filocamo, C. Traboni, A. Nicosia, R. Cortese, A. Vitelli, The human scavenger receptor class B type I is a novel candidate receptor for the hepatitis C virus. *EMBO J.* **21**, 5017–5025 (2002). doi:10.1093/emboj/cdf529 Medline

12. H. E. Drummer, I. Boo, P. Poumbourios, Mutagenesis of a conserved fusion peptide-like motif and membrane-proximal heptad-repeat region of hepatitis C virus glycoprotein E1. *J. Gen. Virol.* **88**, 1144–1148 (2007). doi:10.1099/vir.0.82567-0 Medline

13. M. T. Catanese, K. Uryu, M. Kopp, T. J. Edwards, L. Andrus, W. J. Rice, M. Silvestry, R. J. Kuhn, C. M. Rice, Ultrastructural analysis of hepatitis C virus particles. *Proc. Natl. Acad. Sci. U.S.A.* **110**, 9505–9510 (2013). doi:10.1073/pnas.1307527110 Medline

14. G. Vieyres, J. Dubuisson, T. Pietschmann, Incorporation of hepatitis C virus E1 and E2 glycoproteins: The keystones on a peculiar virion. *Viruses* **6**, 1149–1187 (2014). doi:10.3390/v6031149 Medline

15. L. Stejskal, W. D. Lees, D. S. Moss, M. Palor, R. J. Bingham, A. J. Shepherd, J. Grove, Flexibility and intrinsic disorder are conserved features of hepatitis C virus E2 glycoprotein. *PLOS Comput. Biol.* **16**, e1007710 (2020). doi:10.1371/journal.pcbi.1007710 Medline

16. M. Lavie, X. Hanoulle, J. Dubuisson, Glycan shielding and modulation of hepatitis C virus neutralizing antibodies. *Front. Immunol.* **9**, 910 (2018). doi:10.3389/fimmu.2018.00910 Medline

17. A. Goffard, N. Callens, B. Bartosch, C. Wychowski, F.-L. Cosset, C. Montpellier, J. Dubuisson, Role of N-linked glycans in the functions of hepatitis C virus envelope glycoproteins. *J. Virol.* **79**, 8400–8409 (2005). doi:10.1128/JVI.79.13.8400-8409.2005 Medline

18. J. Prentoe, R. Velázquez-Moctezuma, E. H. Augestad, A. Galli, R. Wang, M. Law, H. Alter, J. Bukh, Hypervariable region 1 and N-linked glycans of hepatitis C regulate virion neutralization by modulating envelope conformations. *Proc. Natl. Acad. Sci. U.S.A.* **116**, 10039–10047 (2019). doi:10.1073/pnas.1822002116 Medline

19. L. Kong, E. Giang, T. Nieusma, R. U. Kadam, K. E. Cogburn, Y. Hua, X. Dai, R. L. Stanfield, D. R. Burton, A. B. Ward, I. A. Wilson, M. Law, Hepatitis C virus E2 envelope glycoprotein core structure. *Science* **342**, 1090–1094 (2013). doi:10.1126/science.1243876 Medline

20. I. Khan, D. S. Katikaneni, Q. Han, L. Sanchez-Felipe, K. Hanada, R. L. Ambrose, J. M. Mackenzie, K. V. Konan, Modulation of hepatitis C virus genome replication by glycosphingolipids and four-phosphate adaptor protein 2. *J. Virol.* **88**, 12276–12295 (2014). doi:10.1128/JVI.00970-14 Medline

21. A. I. Flyak, S. Ruiz, M. D. Colbert, T. Luong, J. E. Crowe Jr., J. R. Bailey, P. J. Bjorkman, HCV broadly neutralizing antibodies use a CDRH3 disulfide motif to recognize an E2 glycoprotein site that can be targeted for vaccine design. *Cell Host Microbe* **24**, 703–716.e3 (2018). doi:10.1016/j.chom.2018.10.009 Medline

22. N. Tzarum, E. Giang, L. Kong, L. He, J. Prentoe, E. Augestad, Y. Hua, S. Castillo, G. M. Lauer, J. Bukh, J. Zhu, I. A. Wilson, M. Law, Genetic and structural insights into broad

neutralization of hepatitis C virus by human V_H1-69 antibodies. *Sci. Adv.* **5**, eaav1882 (2019). doi:10.1126/sciadv.aav1882 Medline

23. N. Tzarum, I. A. Wilson, M. Law, The neutralizing face of hepatitis C virus E2 envelope glycoprotein. *Front. Immunol.* **9**, 1315 (2018). doi:10.3389/fimmu.2018.01315 Medline

24. A. Kumar, R. A. Hossain, S. A. Yost, W. Bu, Y. Wang, A. D. Dearborn, A. Grakoui, J. I. Cohen, J. Marcotrigiano, Structural insights into hepatitis C virus receptor binding and entry. *Nature* **598**, 521–525 (2021). doi:10.1038/s41586-021-03913-5 Medline

25. K. El Omari, O. Iourin, J. Kadlec, G. Sutton, K. Harlos, J. M. Grimes, D. I. Stuart, Unexpected structure for the N-terminal domain of hepatitis C virus envelope glycoprotein E1. *Nat. Commun.* **5**, 4874 (2014). doi:10.1038/ncomms5874 Medline

26. J. A. Potter, A. M. Owsianka, N. Jeffery, D. J. Matthews, Z.-Y. Keck, P. Lau, S. K. H. Foung, G. L. Taylor, A. H. Patel, Toward a hepatitis C virus vaccine: The structural basis of hepatitis C virus neutralization by AP33, a broadly neutralizing antibody. *J. Virol.* **86**, 12923–12932 (2012). doi:10.1128/JVI.02052-12 Medline

27. L. Kong, R. U. Kadam, E. Giang, T. B. Ruwona, T. Nieusma, J. C. Culhane, R. L. Stanfield, P. E. Dawson, I. A. Wilson, M. Law, Structure of hepatitis C virus envelope glycoprotein E1 antigenic site 314-324 in complex with antibody IGH526. *J. Mol. Biol.* **427**, 2617–2628 (2015). doi:10.1016/j.jmb.2015.06.012 Medline

28. E. Giang, M. Dorner, J. C. Prentoe, M. Dreux, M. J. Evans, J. Bukh, C. M. Rice, A. Ploss, D. R. Burton, M. Law, Human broadly neutralizing antibodies to the envelope glycoprotein complex of hepatitis C virus. *Proc. Natl. Acad. Sci. U.S.A.* **109**, 6205–6210 (2012). doi:10.1073/pnas.1114927109 Medline

29. T. B. Ruwona, E. Giang, T. Nieusma, M. Law, Fine mapping of murine antibody responses to immunization with a novel soluble form of hepatitis C virus envelope glycoprotein complex. *J. Virol.* **88**, 10459–10471 (2014). doi:10.1128/JVI.01584-14 Medline

30. L. Cao, B. Yu, D. Kong, Q. Cong, T. Yu, Z. Chen, Z. Hu, H. Chang, J. Zhong, D. Baker, Y. He, Functional expression and characterization of the envelope glycoprotein E1E2 heterodimer of hepatitis C virus. *PLOS Pathog.* **15**, e1007759 (2019). doi:10.1371/journal.ppat.1007759 Medline

31. J. D. Guest, R. Wang, K. H. Elkholy, A. Chagas, K. L. Chao, T. E. Cleveland IV, Y. C. Kim, Z.-Y. Keck, A. Marin, A. S. Yunus, R. A. Mariuzza, A. K. Andrianov, E. A. Toth, S. K. H. Foung, B. G. Pierce, T. R. Fuerst, Design of a native-like secreted form of the hepatitis C virus E1E2 heterodimer. *Proc. Natl. Acad. Sci. U.S.A.* **118**, e2015149118 (2021). doi:10.1073/pnas.2015149118 Medline

32. X. V. Thomas, B. P. X. Grady, J. T. M. Van Der Meer, C. K. Ho, J. W. Vanhommerig, S. P. Rebers, M. D. De Jong, M. Van Der Valk, M. Prins, R. Molenkamp, J. Schinkel, MOSAIC (MSM Observational Study of Acute Infection with hepatitis C) study group, Genetic characterization of multiple hepatitis C virus infections following acute infection in HIV-infected men who have sex with men. *AIDS* **29**, 2287–2295 (2015). doi:10.1097/QAD.0000000000000838 Medline

33. B. G. Pierce, Z.-Y. Keck, P. Lau, C. Fauvelle, R. Gowthaman, T. F. Baumert, T. R. Fuerst, R. A. Mariuzza, S. K. H. Foung, Global mapping of antibody recognition of the hepatitis C

virus E2 glycoprotein: Implications for vaccine design. *Proc. Natl. Acad. Sci. U.S.A.* **113**, E6946–E6954 (2016). doi:10.1073/pnas.1614942113 Medline

34. S. J. Merat, R. Molenkamp, K. Wagner, S. M. Koekkoek, D. van de Berg, E. Yasuda, M. Böhne, Y. B. Claassen, B. P. Grady, M. Prins, A. Q. Bakker, M. D. de Jong, H. Spits, J. Schinkel, T. Beaumont, Hepatitis C virus broadly neutralizing monoclonal antibodies isolated 25 years after spontaneous clearance. *PLOS ONE* **11**, e0165047 (2016). doi:10.1371/journal.pone.0165047 Medline

35. M. L. Carlson, J. W. Young, Z. Zhao, L. Fabre, D. Jun, J. Li, J. Li, H. S. Dhupar, I. Wason, A. T. Mills, J. T. Beatty, J. S. Klassen, I. Rouiller, F. Duong, The Peptidisc, a simple method for stabilizing membrane proteins in detergent-free solution. *eLife* **7**, e34085 (2018). doi:10.7554/eLife.34085 Medline

36. J. C. Meunier, R. S. Russell, V. Goossens, S. Priem, H. Walter, E. Depla, A. Union, K. N. Faulk, J. Bukh, S. U. Emerson, R. H. Purcell, Isolation and characterization of broadly neutralizing human monoclonal antibodies to the e1 glycoprotein of hepatitis C virus. *J. Virol.* **82**, 966–973 (2008). doi:10.1128/JVI.01872-07 Medline

37. W. Schaefer, J. T. Regula, M. Bähner, J. Schanzer, R. Croasdale, H. Dürr, C. Gassner, G. Georges, H. Kettenberger, S. Imhof-Jung, M. Schwaiger, K. G. Stubenrauch, C. Sustmann, M. Thomas, W. Scheuer, C. Klein, Immunoglobulin domain crossover as a generic approach for the production of bispecific IgG antibodies. *Proc. Natl. Acad. Sci. U.S.A.* **108**, 11187–11192 (2011). doi:10.1073/pnas.1019002108 Medline

38. A. Punjani, D. J. Fleet, 3D variability analysis: Resolving continuous flexibility and discrete heterogeneity from single particle cryo-EM. *J. Struct. Biol.* **213**, 107702 (2021). doi:10.1016/j.jsb.2021.107702 Medline

39. M. Castelli, N. Clementi, G. A. Sautto, J. Pfaff, K. M. Kahle, T. Barnes, B. J. Doranz, M. Dal Peraro, M. Clementi, R. Burioni, N. Mancini, HCV E2 core structures and mAbs: Something is still missing. *Drug Discov. Today* **19**, 1964–1970 (2014). doi:10.1016/j.drudis.2014.08.011 Medline

40. A. Wahid, F. Helle, V. Descamps, G. Duverlie, F. Penin, J. Dubuisson, Disulfide bonds in hepatitis C virus glycoprotein E1 control the assembly and entry functions of E2 glycoprotein. *J. Virol.* **87**, 1605–1617 (2013). doi:10.1128/JVI.02659-12 Medline

41. T. Krey, J. d'Alayer, C. M. Kikuti, A. Saulnier, L. Damier-Piolle, I. Petitpas, D. X. Johansson, R. G. Tawar, B. Baron, B. Robert, P. England, M. A. A. Persson, A. Martin, F. A. Rey, The disulfide bonds in glycoprotein E2 of hepatitis C virus reveal the tertiary organization of the molecule. *PLOS Pathog.* **6**, e1000762 (2010). doi:10.1371/journal.ppat.1000762 Medline

42. M. Q. Marín, K. Sliepen, J. García-Arriaza, S. M. Koekkoek, P. Pérez, C. Ó. S. Sorzano, C. E. Gómez, R. W. Sanders, M. Esteban, Optimized hepatitis C virus (HCV) E2 glycoproteins and their immunogenicity in combination with MVA-HCV. *Vaccines* **8**, 440 (2020). doi:10.3390/vaccines8030440 Medline

43. W. Wang, M. Guan, Y. Liu, Q. Xu, H. Peng, X. Liu, Z. Tang, Y. Zhu, D. Wu, H. Ren, P. Zhao, Z. Qi, Alanine scanning mutagenesis of hepatitis C virus E2 cysteine residues: Insights into E2 biogenesis and antigenicity. *Virology* **448**, 229–237 (2014). doi:10.1016/j.virol.2013.10.020 Medline

44. V. Deleersnyder, A. Pillez, C. Wychowski, K. Blight, J. Xu, Y. S. Hahn, C. M. Rice, J. Dubuisson, Formation of native hepatitis C virus glycoprotein complexes. *J. Virol.* **71**, 697–704 (1997). doi:10.1128/jvi.71.1.697-704.1997 Medline

45. J. M. Pfaff-Kilgore, E. Davidson, K. Kadash-Edmondson, M. Hernandez, E. Rosenberg, R. Chambers, M. Castelli, N. Clementi, N. Mancini, J. R. Bailey, J. E. Crowe Jr., M. Law, B. J. Doranz, Sites of vulnerability in HCV E1E2 identified by comprehensive functional screening. *Cell Rep.* **39**, 110859 (2022). doi:10.1016/j.celrep.2022.110859 Medline

46. C. Di Lorenzo, A. G. N. Angus, A. H. Patel, Hepatitis C virus evasion mechanisms from neutralizing antibodies. *Viruses* **3**, 2280–2300 (2011). doi:10.3390/v3112280 Medline

47. J. C. Meunier, A. Fournillier, A. Choukhi, A. Cahour, L. Cocquerel, J. Dubuisson, C. Wychowski, Analysis of the glycosylation sites of hepatitis C virus (HCV) glycoprotein E1 and the influence of E1 glycans on the formation of the HCV glycoprotein complex. *J. Gen. Virol.* **80**, 887–896 (1999). doi:10.1099/0022-1317-80-4-887 Medline

48. G. Vieyres, X. Thomas, V. Descamps, G. Duverlie, A. H. Patel, J. Dubuisson, Characterization of the envelope glycoproteins associated with infectious hepatitis C virus. *J. Virol.* **84**, 10159–10168 (2010). doi:10.1128/JVI.01180-10 Medline

49. L. Cocquerel, S. Duvet, J.-C. Meunier, A. Pillez, R. Cacan, C. Wychowski, J. Dubuisson, The transmembrane domain of hepatitis C virus glycoprotein E1 is a signal for static retention in the endoplasmic reticulum. *J. Virol.* **73**, 2641–2649 (1999). doi:10.1128/JVI.73.4.2641-2649.1999 Medline

50. R. Gopal, K. Jackson, N. Tzarum, L. Kong, A. Ettenger, J. Guest, J. M. Pfaff, T. Barnes, A. Honda, E. Giang, E. Davidson, I. A. Wilson, B. J. Doranz, M. Law, Probing the antigenicity of hepatitis C virus envelope glycoprotein complex by high-throughput mutagenesis. *PLOS Pathog.* **13**, e1006735 (2017). doi:10.1371/journal.ppat.1006735 Medline

51. J. P. Michalak, C. Wychowski, A. Choukhi, J. C. Meunier, S. Ung, C. M. Rice, J. Dubuisson, Characterization of truncated forms of hepatitis C virus glycoproteins. *J. Gen. Virol.* **78**, 2299–2306 (1997). doi:10.1099/0022-1317-78-9-2299 Medline

52. J. Patel, A. H. Patel, J. McLauchlan, The transmembrane domain of the hepatitis C virus E2 glycoprotein is required for correct folding of the E1 glycoprotein and native complex formation. *Virology* **279**, 58–68 (2001). doi:10.1006/viro.2000.0693 Medline

53. M. Brazzoli, A. Helenius, S. K. H. Foung, M. Houghton, S. Abrignani, M. Merola, Folding and dimerization of hepatitis C virus E1 and E2 glycoproteins in stably transfected CHO cells. *Virology* **332**, 438–453 (2005). doi:10.1016/j.virol.2004.11.034 Medline

54. J. S. McLellan, M. Chen, S. Leung, K. W. Graepel, X. Du, Y. Yang, T. Zhou, U. Baxa, E. Yasuda, T. Beaumont, A. Kumar, K. Modjarrad, Z. Zheng, M. Zhao, N. Xia, P. D. Kwong, B. S. Graham, Structure of RSV fusion glycoprotein trimer bound to a prefusion-specific neutralizing antibody. *Science* **340**, 1113–1117 (2013). doi:10.1126/science.1234914 Medline

55. S. W. de Taeye, G. Ozorowski, A. Torrents de la Peña, M. Guttman, J.-P. Julien, T. L. G. M. van den Kerkhof, J. A. Burger, L. K. Pritchard, P. Pugach, A. Yasmeen, J. Crampton, J. Hu, I. Bontjer, J. L. Torres, H. Arendt, J. DeStefano, W. C. Koff, H. Schuitemaker, D. Eggink, B. Berkhout, H. Dean, C. LaBranche, S. Crotty, M. Crispin, D. C. Montefiori, P.

J. Klasse, K. K. Lee, J. P. Moore, I. A. Wilson, A. B. Ward, R. W. Sanders, Immunogenicity of stabilized HIV-1 envelope trimers with reduced exposure of non-neutralizing epitopes. *Cell* **163**, 1702–1715 (2015). doi:10.1016/j.cell.2015.11.056 Medline

56. J. Juraszek, L. Rutten, S. Blokland, P. Bouchier, R. Voorzaat, T. Ritschel, M. J. G. Bakkers, L. L. R. Renault, J. P. M. Langedijk, Stabilizing the closed SARS-CoV-2 spike trimer. *Nat. Commun.* **12**, 244 (2021). doi:10.1038/s41467-020-20321-x Medline

57. J. H. Lee, G. Ozorowski, A. B. Ward, Cryo-EM structure of a native, fully glycosylated, cleaved HIV-1 envelope trimer. *Science* **351**, 1043–1048 (2016). doi:10.1126/science.aad2450 Medline

58. P. Falson, B. Bartosch, K. Alsaleh, B. A. Tews, A. Loquet, Y. Ciczora, L. Riva, C. Montigny, C. Montpellier, G. Duverlie, E.-I. Pécheur, M. le Maire, F.-L. Cosset, J. Dubuisson, F. Penin, Hepatitis C virus envelope glycoprotein E1 forms trimers at the surface of the virion. *J. Virol.* **89**, 10333–10346 (2015). doi:10.1128/JVI.00991-15 Medline

59. P. Emsley, M. Crispin, Structural analysis of glycoproteins: Building N-linked glycans with Coot. *Acta Crystallogr. D Struct. Biol.* **74**, 256–263 (2018). doi:10.1107/S2059798318005119 Medline